J. Fluid Mech. (1996), *vol.* 308, *pp.* 63–96

The effect of counterflow on the development of compressible shear layers

By P. J. STRYKOWSKI[1], A. KROTHAPALLI[2] AND S. JENDOUBI[1]

[1] Department of Mechanical Engineering, University of Minnesota, Minneapolis, MN 55455, USA

[2] Department of Mechanical Engineering, Florida A&M University and Florida State University, Tallahassee, FL 32316, USA

(Received 24 January 1995 and in revised form 27 September 1995)

A compressible countercurrent shear layer was investigated experimentally by establishing reverse flow around the perimeter of a supersonic jet. Measurements demonstrate that spatial growth rates of the countercurrent shear layer significantly exceed those of the classical coflowing layer at comparable density ratios and levels of compressibility. Experiments also reveal the presence of coherent three-dimensional structures in the countercurrent shear layer at convective Mach numbers where similar structures are not present in coflowing layers. It is argued that these kinematic differences are responsible for the enhanced diffusion of the shear layer with counterflow. The spatio-temporal theory is used to examine the connection between the experimental observations and the existence of a transition from convective to absolute instability in high-speed shear layers.

1. Introduction

The experimental work of Papamoschou & Roshko (1988), which examined the effect of compressibility on free shear layer mixing, launched one of the most extensive examinations by the fluid dynamics research community in the last decade. Although Bogdanoff (1983) and Chinzei *et al.* (1986) considered the unique role of compressibility somewhat earlier – proposing a unifying parameter later called the convective Mach number – the experiments of Papamoschou & Roshko isolated the effect of compressibility from the other important parameters including density ratio, velocity ratio, and specific heat ratio. Their research quantified a rather disturbing trend, which was observed much earlier and reported in the work of Birch & Eggers (1973), namely that mixing is significantly suppressed as the convective Mach number is increased. This effect motivated a plethora of research in the area owing to the considerable impact it has on the design of high-speed devices such as supersonic combustion chambers, as well as the need to reduce the noise emission from supersonic jet exhaust.

A complete physical explanation for the suppressed mixing behaviour of compressible shear layers remains elusive. Experimental studies by Papamoschou (1989), Fourguette, Mungal & Dibble (1991), Messersmith, Dutton & Krier (1991), Clemens & Mungal (1992) and Samimy, Reeder & Elliott (1992) support the fundamental observation that the precipitous decrease in mixing with increasing compressibility is accompanied by a distinct absence of coherent two-dimensional structure in the shear layer. The importance of these structures in achieving efficient entrainment between dissimilar streams and thereby increased growth rates was first

elucidated in high-speed flows by Brown & Roshko (1974). Concomitant with the reduction in the cross-stream extent of the large-scale structures is a three-dimensional transition characterized by a limited spanwise coherence in the flow. Detailed turbulence measurements obtained using non-intrusive techniques (Samimy, Erwin & Elliot, 1989; Elliot & Samimy 1990; Goebel & Dutton 1991) further support these observations, indicating a reduction in the cross-stream turbulent transport which is responsible for inhibiting the energy transfer from the mean flow.

The work of Gropengiesser (1970) provides insight into the mechanism responsible for the reduced rates of mixing at elevated Mach numbers. In a single-stream mixing layer Gropengiesser identified an abrupt reduction in the maximum spatial amplification rate when the Mach number of the primary stream was increased; at very high Mach numbers the growth rate was seen to asymptote to a constant non-zero value. More recent studies of the linear spatial theory by Jackson & Grosch (1989) and Sandham & Reynolds (1990) indicate that oblique waves become increasingly amplified relative to plane-wave disturbances as the convective Mach number is increased. Three-dimensional direct simulations of the Navier–Stokes equations by Sandham & Reynolds (1991) corroborate the importance of oblique waves with increasing levels of compressibility and point to the redistribution of vorticity as the primary cause of flow structures described as being elongated in the streamwise direction.

Underpinning the fundamental examination of compressible shear layers is the need to develop efficient strategies for mixing augmentation. Research in this area parallels to a significant extent mixing enhancement studies performed in subsonic flow. Owing to the convectively unstable nature of compressible shear flows, passive control approaches often involve the introduction of artificial disturbances which lead to higher total amplification and significant coherent structure in the flow. Examples of such passive schemes include the use of tabs and streamwise vortex generators, examined in the content of supersonic axisymmetric jets by Samimy, Zaman & Reeder (1991) and Yu *et al.* (1992), as well as a variety of three-dimensional perturbations such as saw-toothed edges and trip wires (Papamoschou 1989). In a similar spirit, various studies have considered the influence of geometric changes on disturbance amplification rates such as the use of elliptic and rectangular cross-sectioned nozzles (Gutmark, Schadow & Wilson 1991). Shock waves have also been used to augment free shear layer mixing as shown in the work of Samimy *et al.* (1989), Shau & Dolling (1989), Clemens & Mungal (1992) and Shau, Dolling & Choi (1993).

Although passive control schemes for supersonic mixing enhancement enjoy reasonable success compared to active control scenarios – which require excessive energy input in high-speed applications (Raman, Rice & Mankbadi 1988; Lepicovsky *et al.* 1988) – continued research in this area is required owing to the losses associated with many of these techniques. A promising approach for the diffusion of compressible shear flows utilizes the efficient energy transfer between the mean and turbulent velocity fields caused by global flow instabilities. One such phenomenon, known as screech, is not new (Powell 1953), but exemplifies the dramatic effect that a self-sustained feedback loop can play in the global flow response (Krothapalli *et al.* 1986). Similar feedback effects involving cavities and wake defects have been explored in the context of supersonic jets by Yu, Gutmark & Schadow (1993) and indicate that significant entrainment can be achieved at high levels of compressibility. In the present study we will examine how alterations in the local velocity field can be used to excite inherent instabilities of the compressible shear layer and thereby achieve a global flow response conducive to the rapid diffusion of the flow. This approach is based on the

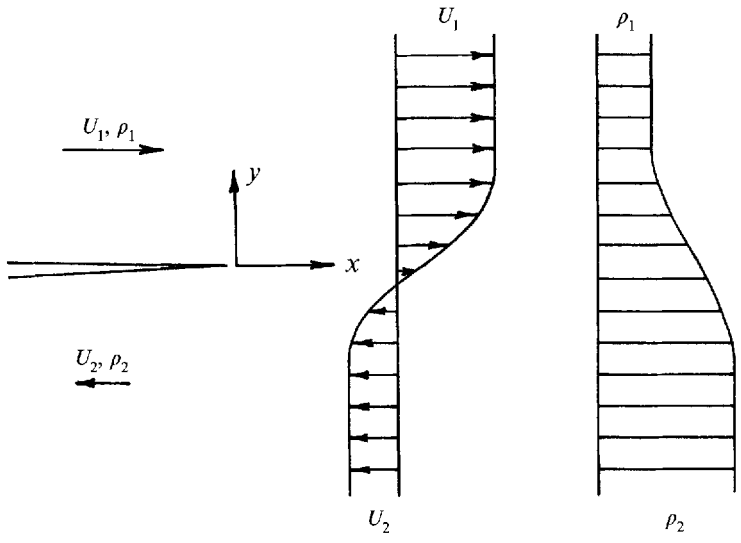

FIGURE 1. A countercurrent shear layer of variable density.

unique stability characteristics of the *countercurrent mixing layer* which will be described in detail in §2. Our discussion will continue in §3 with an overview of the experiment facilities and in §4 with the basic observations of the flow field. Shear layer growth rates will be presented in §5 together with a discussion of the effects of density ratio and convective Mach number. We will provide in §6 some theoretical framework linking the experimental results and linear stability theory, and summarize the work in §7.

2. Countercurrent mixing layers

Spatially developing mixing layers have been the focus of extensive research for decades. This research has examined a vast parameter space including the effects of density ratio, velocity ratio, and compressibility on the mixing layer dynamics, as well as the important role that initial conditions play on the shear layer evolution. However, despite this extraordinary attention, shear layer research has been limited essentially to a broad class of *coflowing* mixing layers produced when dissimilar streams combine downstream of a splitter plate and travel in a common direction as seen in a reference frame fixed with respect to the plate.

Consider now the situation which arises when two nominally parallel streams travel in opposite directions relative to a dividing plate creating a *countercurrent* mixing layer. This configuration is fundamental to all separated flows, but has received relatively little attention in the literature. The countercurrent mixing layer is defined in figure 1 as seen in a coordinate frame fixed at the trailing edge of the plate. The primary flow is represented by the free-stream velocity U_1 and density ρ_1. A secondary stream having free-stream quantities U_2 and ρ_2 is generated and travels in the direction opposite to the primary flow. Parameters affecting the streamwise evolution of the compressible countercurrent mixing layer include the velocity ratio $r \equiv U_2/U_1$, the density ratio $s \equiv \rho_2/\rho_1$, and the convective Mach number $M_c \equiv (U_1 - U_2)/(a_1 + a_2)$, where the subscripts 1 and 2 denote the primary and secondary streams, respectively, and a represents the speed of sound in the free stream; here it is assumed that the specific heat ratio across

the layer is nominally constant. Not unlike the coflowing mixing layer, we expect that the countercurrent shear layer will be influenced by the boundary conditions imposed at the trailing edge of the plate, in particular the disturbance levels and spectral distributions residing in the boundary layer and free streams, as well as the inherent three-dimensionality of the base flow. It is also important to remember that the typical two-dimensional mixing layer studied in the laboratory develops spatially where the streamwise and cross-stream extents of the velocity field U_1 and U_2 are finite.

Temporal countercurrent mixing layers were systematically examined by Thorpe (1968, 1971) and Ramshankar (1988) using a novel tilting tank to create spatially invariant mixing layers of variable density. Their research successfully identified the nature of instability of a one-dimensional mixing region from the growth of the incipient disturbances leading to vortex roll-up and subsequent violent breakdown to turbulence. The work of Ramshankar was particularly elegant, allowing the identification of the fractal nature of the nonlinear vortex evolution due to the absence of a disturbance convection velocity in the laboratory reference frame. In sharp contrast to the temporally evolving shear layers studied by Thorpe and Ramshankar, we were interested in examining a spatially and temporally developing countercurrent layer which would occur, for instance, in the presence of flow separation. One would expect that this complicated flow field may support both upstream and downstream amplifying disturbances and hence the possibility of self-excitation. Humphrey & Li (1981) designed a facility specifically to examine this unique flow field using a dual-contraction wind tunnel, but were unable to avoid a global instability of their facility leading to a large free stagnation region.

Strykowski & Niccum (1991) were the first to systematically investigate the spatially developing countercurrent mixing layer through a series of experiments performed in an incompressible axisymmetric jet ($M_c = 0$) of constant density ($s = 1$). The uniform velocity of the free jet served as the primary stream U_1 and a secondary flow created around the periphery of the primary jet formed the counterflowing stream U_2. For modest amounts of counterflow Strykowski & Niccum demonstrated that disturbance amplification rates scaled proportionally to the velocity ratio defined as $(U_1 - U_2)/(U_1 + U_2)$ as predicted by the linear spatial theory for coflowing mixing layers (Ho & Huerre 1984). When counterflow was increased above a critical level given by $r_{cr} = -0.14$ the mixing layer displayed discrete oscillations resulting in disturbance levels nearly an order of magnitude higher than those predicted by the spatial theory alone; the shear layer response to counterflow below r_{cr} was shown to be analogous to the externally forced mixing layer investigated by Freymuth (1966).

Strykowski & Niccum argued that the transition observed experimentally at r_{cr} was a consequence of global self-excitation of the shear layer due to a transition from convective to absolute instability, which is predicted by spatio-temporal theory to occur at $r_{cr} = -0.136$ in a mixing layer having $s = 1$ and $M_c = 0$ (Huerre & Monkewitz 1985). Subsequent work (Strykowski & Niccum 1992) explored this connection further in a variable-density mixing layer where theoretical predictions of r_{cr} display a strong dependence on the density ratio s. By introducing sulphur hexafluoride into the primary stream, density ratios between approximately 0.2 and 1 were examined in the presence of counterflow. Flow visualization was used to identify critical velocity ratios which varied between -0.14 in the constant-density mixing layer ($s = 1$) to values as small as -0.5 in the mixing layer at the lowest density ratio ($s = 0.196$); note that lower r-values indicate increasing levels of counterflow. These observations were in close agreement with the predicted convective–absolute transition found by Pavithran & Redekopp (1989) over the range of density ratios studied. Strykowski & Niccum also

identified a distinct three-dimensionality of the flow at velocity ratios below r_{cr} giving rise to well-defined streamwise structures in the mixing layer.

The connection between the theoretical concept of absolute instability and global self-excitation, which is documented in the laboratory, is often only circumstantial in nature. Notwithstanding this limitation, many studies have provided convincing evidence that local stability concepts can be effectively exploited to achieve global flow control. For instance, Mathis, Provansal & Boyer (1984) identified the formation of vortex shedding behind bluff bodies with a self-excited global mode in the wake, which is consistent with the local stability models proposed by Koch (1985) and Huerre & Monkewitz (1985). Strykowski (1986) later showed that local alterations in the flow could significantly effect the global wake development. Observations of self-excited vortical structure in low-density jets by Sreenivasan, Raghu & Kyle (1989), Monkewitz *et al.* (1990) and Kyle & Sreenivasan (1993) indicate the dramatic changes brought about by alterations in the density field; agreement between experimental observations and theoretical predictions of the onset of absolute instability from Monkewitz & Sohn (1988) are remarkable.

Global flow self-excitation in weakly diverging flows depends upon the streamwise scale supporting absolute instability (Chomaz, Huerre & Redekopp 1988; Monkewitz 1988). In the context of the countercurrent mixing layer, practical considerations limit the streamwise extent over which the reverse stream U_2 can be maintained in the laboratory and, consequently, the spatial domain of absolutely unstable flow. Experiments of Strykowski & Wilcoxon (1993) explored the relationship between the global jet response to counterflow and the streamwise domain of absolute instability. As the influence of counterflow was extended in the streamwise direction, the wavelength of the global mode increased roughly proportional to $-U_2/U_1$, thereby having a more pronounced affect on the overall jet development as measured, for instance, by increased momentum mixing.

A final observation needs to be emphasized which will serve, in part, to motivate the present investigation. One of the most important attributes of self-excited flows is their inherent insensitivity to externally applied forcing (Huerre & Monkewitz 1990) which, in practical systems, will be imposed by the naturally high levels of background turbulence. In the context of jets, we would like to explore the possibility of whether counterflow can be used to alter the jet behaviour from that of a purely spatial amplifier – which would then depend quite critically on the external forcing – to one having sufficient feedback to support self-excitation. To have a lasting impact in the context of high-speed jet control, the self-excitation must lead to significant nonlinear interaction with the mean flow resulting in enhanced rates of jet diffusion. Therefore, we believe a realistic strategy for shear flow control can exploit the inherent instabilities by modification of the base flow leading to finite regions of absolute instability. In this paper we will examine the extent to which these concepts can be extended beyond the relatively low Reynolds number conditions reported above to realistic jet operating conditions. In particular, we will consider the utility of counterflow control applied to the challenging problem of mixing enhancement in a supersonic jet at Mach 2.

3. Jet facilities and instrumentation

The experiments were conducted in the blow-down compressed-air facility of the Fluid Mechanics Laboratory at Florida State University. The facility is driven by a high-displacement reciprocating air compressor which is capable of supplying air at a maximum storage pressure of 2300 p.s.i.g. The air delivered to the storage tanks is

passed through a series of dryers to reduce absolute humidity prior to expansion through the valve assembly and isentropic nozzle; the maximum relative humidity of the primary air stream exiting the nozzle at Mach 2 (occurring under cold jet operating conditions) was estimated to be less than 50%. Large storage tanks provide a total capacity of 10 m^3 and are capable of driving the Mach 2 primary jet flow examined in this study continuously for up to 30 min. After leaving the storage tanks the air can be heated by passing through an array of resistive tank heaters having a maximum power output of 450 kW and capable of achieving stagnation temperatures in excess of 715 K. Operating the facility at elevated stagnation temperatures requires preheating the facility downstream of the tank heaters. This process bleeds the storage tanks somewhat, but the overall run time is not significantly affected owing to the concomitant reduction in the mass flow rate with increasing stagnation temperature. The stagnation pressure was held invariant to within 0.5% of its nominal value during each experiment using staged control valves.

For the present investigation the blow-down facility was fitted with an axisymmetric converging–diverging nozzle designed by the method of characteristics for operation at Mach 2; the diameter D of the nozzle in the exit plane was 29.2 mm. All experiments were performed at the design Mach 2 isentropic pressure ratio defined between the plenum stagnation pressure $p_{t,1}$ and the static pressure in the jet exit plane. To achieve a reasonable operating range in terms of convective Mach number, experiments were performed at primary stagnation temperatures $T_{t,1}$ between 300 and 715 K. The cold supersonic jet ($T_{t,1} = 300$ K) issuing from the nozzle at a Reynolds number $Re_D = 2.8 \times 10^6$, served as the primary stream U_1. The conditions of the free shear layers emanating from the nozzle lip were defined by the velocity ratio r, density ratio s, and convective Mach number M_c. In the case of the cold free jet issuing into quiescent fluid ($U_2 = 0$) the velocity ratio was zero, at a density ratio of 0.55, and a convective Mach number of 0.85. In the presence of elevated stagnation temperatures ($T_{t,1} = 715$ K) the convective Mach number of the shear layer was increased to 1.06 at a density ratio of 1.32 in the absence of external flow ($U_2 = 0$). The higher temperature of the primary stream resulted in a reduced exit Reynolds number of $Re_D = 8.8 \times 10^5$. The laboratory conditions into which the supersonic jet exhausted were nominally $T_{t,2} = 300$ K at a relative humidity of 35–40%.

3.1. *Supersonic counterflowing nozzle*

The configuration employed to establish a compressible countercurrent shear layer is shown in figure 2. The uniform exhaust flow of the supersonic jet serves as the primary stream U_1 defined in a reference frame having its origin in the nozzle exit plane ($x = 0$). A collar–manifold assembly is positioned concentrically around the primary nozzle and guides the peripheral secondary stream in the opposite direction to the primary flow, creating a countercurrent shear layer in the region immediately downstream of the jet exit. The driving force behind the secondary flow is a regenerative vacuum system capable of delivering sizable volumetric flow at moderate vacuum pressures. A fixed collar geometry was used for this study as defined in the following parameter space: extension length $L/D = 2.3$; gap width measured in the jet exit plane of $w/D = 0.22$; and a collar divergence half-angle of 9°. Estimates of the counterflowing velocity U_2 were made, assuming uniform flow in the gap of the secondary stream at the origin ($x = 0$), by direct measurement of the mass flow drawn through the manifold system using a laminar flow meter located in the vacuum supply line.

The operation of the counterflowing nozzle requires a simple iterative procedure. Once the vacuum system is activated and the counterflowing stream is established, a

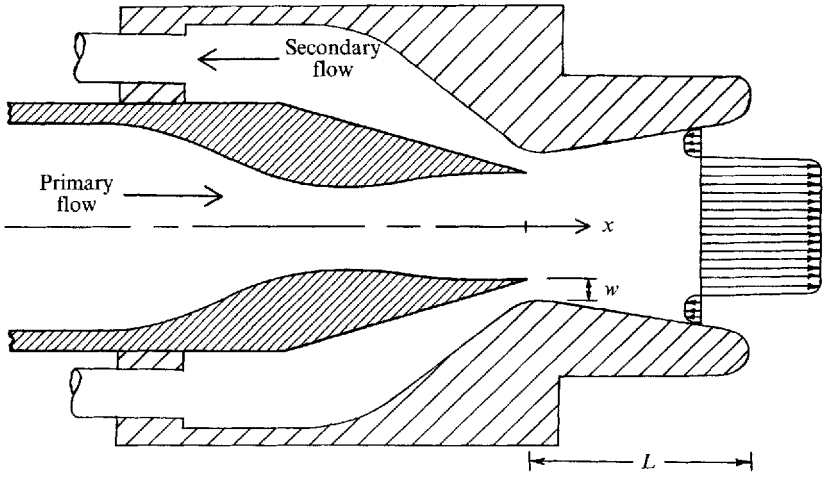

FIGURE 2. Axisymmetric nozzle–collar arrangement used to create counterflow in a supersonic jet.

pressure drop is created along the gap defined by the edge of the primary jet and the collar wall. Consequently, the static pressure measured on the collar surface in the jet exit plane ($x = 0$) is slightly subatmospheric, requiring that the stagnation pressure of the primary stream $p_{t,1}$ be adjusted to achieve the desired isentropic pressure ratio corresponding to a Mach 2 flow exiting the nozzle. This procedure requires some iteration to attain the matched conditions, but provides a relatively wave-free flow as will be shown in the discussion to follow. The velocity ratio of the countercurrent shear layer within the collar serves as the principal control parameter in this study. For the geometry of figure 2, the velocity ratio is defined by the values of the primary velocity U_1 and secondary velocity U_2 as measured in the jet exit plane at $x = 0$.

3.2. *Instrumentation*

Pitot probe surveys were conducted to quantify the spreading rate of the mixing layer as a function of velocity ratio. A total pressure probe having an inner diameter of 0.5 mm was rigidly fixed to a Daedal three-dimensional traversing system with a spatial resolution of 10^{-5} m. Time-integrated pressure measurements were obtained using Validyne pressure transducers digitized at 12-bit resolution and sampled for 1.2 s. Radial and azimuthal Pitot profiles were also used to periodically realign the traverse with the true jet axis, a necessary procedure owing to the expansion of the facility over extended periods of operation caused by heating. Fluctuating pressures were measured in the compressible shear layer by mounting a fast-response Kulite pressure transducer with an effective sensor area of 1.6 mm in diameter into the tip of a conventional total head probe. The frequency response of the transducer was found to be flat within 5% up to 60 kHz; the fluctuating pressure signals were analogue low-pass filtered at 60 kHz and amplified to optimize the A/D converter.

Visualization of the jet was achieved by creating laser sheet images of the axial and diametral planes of the jet axis using a pair of Spectra Physics frequency-doubled Nd:YAG pulsed lasers. The lasers were fired simultaneously with a pulse energy of approximately 90 mJ each and a pulse width of 11 ns (10 Hz repetition rate), effectively freezing the flow and providing non-intrusive and non-integrated images of the large structures. Fine condensation particles formed in the mixing region between the dry cold gas of the primary jet and the relatively moist ambient air were used for light

scattering based on the product formation technique described by Clemens & Mungal (1991). At the operating conditions of the cold Mach 2 free jet ($T_{t,1} = 300$ K), the exit velocity was 520 m s^{-1} at a static temperature of 170 K. A representative time scale of the flow was estimated to be $\tau_f = 20$ μs using the shear layer Pitot thickness as the relevant length scale. Direct measurements of the condensed droplet diameters were not made, but conservative estimates from Fourguette *et al.* (1991) and Clemens & Mungal under similar conditions indicate values less than 0.3 μm. Based on this value the particle time scale was computed as $\tau_p = 0.3$ μs, providing a Stokes number τ_p/τ_f of the order of 0.015, which according to the computations of Samimy & Lele (1990) and the experiments of Ross, Lourenco & Krothapilli (1994) is sufficiently small to expect that the particles will accurately capture the flow dynamics.

Since condensation marking was not possible at elevated stagnation temperatures, light scattering in the heated jet ($T_{t,1} = 715$ K) was achieved by seeding the primary flow stream with 0.3 μm aluminium oxide particles. The relevant flow time scale was estimated as $\tau_f = 12$ μs at a jet velocity of 800 m s^{-1} and a static temperature of 400 K. A corresponding particle time constant of $\tau_p = 1$ μs produces a Stokes number of 0.08, which is at least five times larger than the condensation particles, but still significantly less than the criterion proposed by Samimy & Lele (1990) and Ross *et al.* (1994) for accurate flow marking. All images were captured using a Pentax 6 × 7 camera and Kodak professional black and white film.

4. Jet response to counterflow

We begin our discussion with basic observations made in a Mach 2 unheated jet ($T_{t,1} = 300$ K) influenced by counterflow. As described earlier in the context of figure 2, an adverse pressure gradient, as seen by the primary flow U_1, exists owing to the secondary counterflowing stream U_2. The pressure rise within the collar between $x = 0$ and $x = L$ was documented by measuring the local static (gauge) pressure Δp_c along the collar surface. This distribution is shown in figure 3 for the maximum counterflow velocity $|U_2|$ that was studied. The minimum collar pressure, occurring in the jet exit plane, is roughly 3 % of the stagnation pressure of the primary stream $p_{t,1}$ and displays a nearly linear dependence on distance within the collar. To maintain ideally expanded flow in the jet exit plane, $p_{t,1}$ was reduced from the free jet value ($U_2 = 0$) until the desired pressure ratio was achieved. Under these conditions, the magnitudes of the primary and secondary stream velocities at $x = 0$ were 520 m s^{-1} and 65 m s^{-1}, respectively. The corresponding velocity and density ratios defined at the same position were $r = -0.13$ and $s = 0.55$ at a convective Mach number of $M_c = 0.96$.

The global jet behaviour was examined through detailed measurements of Mach number distributions along the jet axis as shown in figure 4. The free jet, defined by the flow when the collar is removed from the primary nozzle, was used as a base of comparison for the counterflow studies. The free jet profile suggests the presence of weak waves in the region immediately downstream of the jet exit. The origin of these waves was found to reside in the nozzle itself, a consequence of subtle imperfections in the tracer lathe used to generate the internal contour. Zapryagaev & Solotchin (1988) and Novopashin & Perepelkin (1989) indicate that 'scratches' as small as 0.2 % of the nozzle exit diameter can cause such perturbations in supersonic jets, indicating the care with which nozzles must be manufactured to minimize finite-amplitude wave generation. Measurements of mixing layer growth rates presented in §5 suggest that these wave effects do not significantly influence the development of the compressible shear layer of the jet, a result which is consistent with the existing literature on the

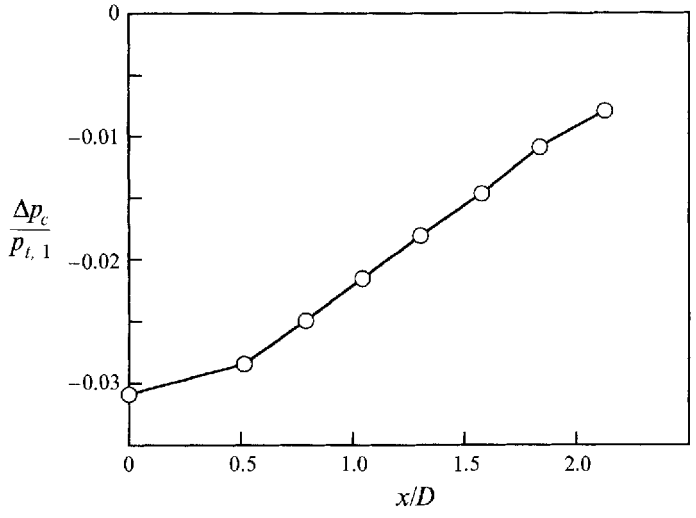

FIGURE 3. Static pressure distribution along the inner collar surface.

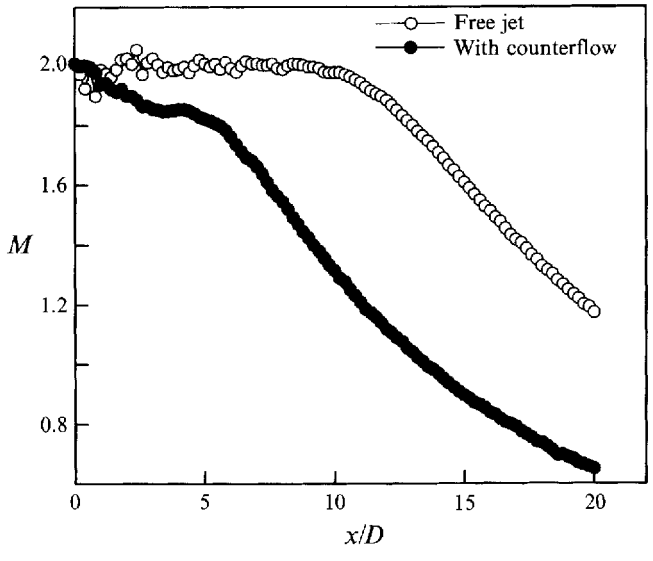

FIGURE 4. Axial Mach number profiles in a free jet and a jet with counterflow.

interaction of shock waves with free shear layers (Samimy *et al.* 1989; Shau *et al.* 1993). The termination of the potential core of the free jet also agrees quite well with existing data for supersonic unheated jets by Scharton, White & Rentz (1973); corresponding data collected in the absence of counterflow but with the collar in place (Strykowski & Krothapalli 1993) indicate that the presence of the collar extension itself has no appreciable impact on the entrainment characteristics of the jet.

An axial Mach profile in the jet at a velocity ratio of $r = -0.13$ is also shown in figure 4 and illustrates the abrupt termination of the potential core at $x/D \approx 5$. The reduction in the core length by a factor of approximately two compared to the free jet is a indication of the dramatic effect of counterflow on jet diffusion. Owing to the adverse pressure gradient in the collar region, the primary stream experiences a deceleration

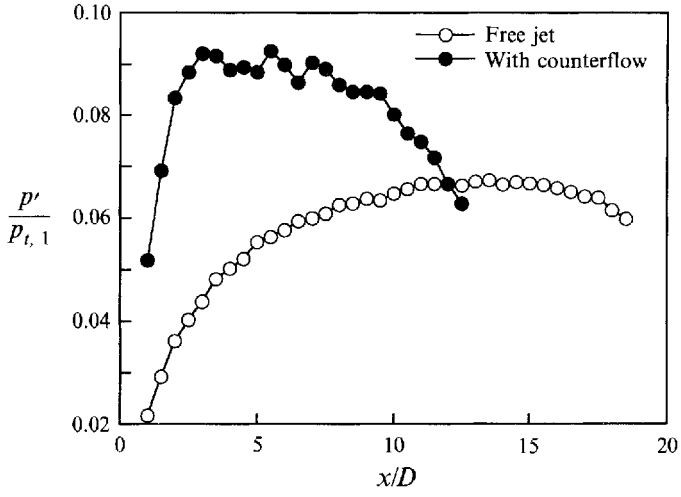

FIGURE 5. Fluctuating pressure profiles in the shear layer of a free jet and a jet with counterflow.

which can be observed over the first 2–3 jet diameters. Total pressure recovery along the potential core indicates that this compression is essentially isentropic resulting in a drop in the centreline Mach number from 2.0 to 1.85. The absence of any noticeable finite-amplitude waves further supports the reversible nature of the deceleration. Downstream of the collar extension a constant-Mach-number region is again observed up to the location where the shear layers merge. The flow deceleration in the jet near field is responsible for a slight elevation in the density ratio from 0.55, in the jet exit plane, to 0.58 in the region between $x = L$ and $x/D \approx 5$. There is a corresponding reduction in the convective Mach number from 0.96 at $x = 0$ to a value of 0.82 in the constant-pressure potential core. At the present time we will continue to define the velocity ratio, density ratio, and convective Mach number in the jet exit plane, and will demonstrate in §5 that the changes in s and M_c alone cannot explain the appreciable diffusion observed in the jet with counterflow.

To provide further insight into the enhanced jet diffusion suggested by the axial Mach number distributions, pressure fluctuations were captured in the shear layer of the jet. A fast-response Kulite pressure transducer mounted in the tip of a total head probe was traversed in the streamwise direction along an iso-Mach line of 1.0. The sonic line was approximately the radial position in the shear layer where the fluctuation level was maximum. This location provided a means of comparing the disturbance levels in the shear layer as a function of the velocity ratio, as well as addressing the issue of flow self-similarity based on turbulence quantities. The ratio of the probe diameter to the local thickness of the mixing layer (to be defined in §5 as the Pitot thickness) varied between $\frac{1}{8}$ and $\frac{1}{10}$ in the region of measurement which extended in the streamwise direction from within the collar to beyond the termination of the potential core. Measuring the maximum value of p' is convenient because it effectively reduces the error caused by a finite probe, since the gradients in p' are smallest at the peak location. The Kulite probe responds very linearly to mean pressures over the usable operating range and provides reliable spectral resolution up to 60 kHz as demonstrated by Shau *et al.* (1993).

The r.m.s. pressure fluctuations normalized by the primary-stream stagnation conditions are presented in figure 5 for the free jet and the counterflowing jet under the conditions described in figure 4 ($r = -0.13$; $s = 0.55$). The disturbances in the

countercurrent shear layer, indicated by the solid symbols, increase rapidly over the first several diameters reaching levels roughly twice those observed in the free jet (open symbols). At the velocity ratio of -0.13 the amplification process is confined to the initial shear layer region within the collar ($x < L$) where significant counterflow can be sustained, downstream of which a saturation level is reached and the velocity ratio approaches zero since $U_2 \approx 0$. Hence, it appears that the initial saturation amplitude is determined by the dynamics of the countercurrent mixing layer and is not affected by the merging of the shear layers due to the finite size of the potential stream U_1. Downstream of the potential core, which terminates at $x/D \approx 5$ in the counterflowing jet, the disturbance level decreases as the mean shear of the jet profile cannot support the levels established in the shear layer. These basic observations are consistent with those of Strykowski & Wilcoxon (1993) obtained from detailed velocity measurements in a subsonic jet with counterflow. In summary, the pressure fluctuations in the shear layer of the free jet display similar trends to the counterflowing jet with the distinct difference being that the absolute level of the disturbances is higher in the latter case. (The spectral content of the far-field pressure fluctuations is also affected by counterflow as recently shown by King, Krothapalli & Strykowski 1995).

Scales on the order of the largest dimensions in the flow – so-called coherent structures – were the distinguishing feature observed by Brown & Roshko (1974) in their seminal work on high-speed shear layers. As described earlier, the absence of coherent structures in highly compressible flows is believed to be a principal cause of suppressed levels of momentum diffusion and entrainment. The elevated disturbance levels and rapid diffusion of the potential core in the jet with counterflow (figures 4 and 5) would imply the presence of coherent structures normally absent at the convective Mach number of this flow ($M_c > 0.8$). A visualization study was conducted to evaluate the nature of the flow structures present under the counterflow conditions currently being discussed where the velocity ratio is -0.13 and the density ratio is 0.55. Planar light scattering from condensation droplets formed in the mixing region between the cold primary stream ($T_{t,1} = 300$ K) and the moist ambient air served to illuminate the structures in the layer; see §3.2 for a description of the technique.

Planar images of the axial centreplane of the jet were obtained by exposing the mixing region to a single laser light pulse of 11 ns duration, effectively freezing the flow; structures can be expected to travel a distance of approximately 3 μm during this exposure. The illuminated shear layers shown in figure 6 extend from the collar at $x/D = 2.3$ to roughly $x/D = 5$. The free jet shear layers (figure 6*a*) display very little organized motion characteristic of high convective Mach number flows (Clemens & Mungal 1992). However, when counterflow is activated (figure 6*b*) the mixing layer structures resemble those seen at significantly lower levels of compressibility and commonly associated with regions of coherent spanwise aligned (azimuthal) vorticity. Observations made from an ensemble of instantaneous photographs taken under nominally identical conditions indicate that mixed fluid often penetrates to the jet centreline at streamwise distances as small as $x/D = 5$ when counterflow is applied. This position is consistent with the axial Mach number distribution shown in figure 4 at $r = -0.13$ where the potential core is seen to terminate. One additional observation which can be made from examining many instantaneous axial plane images is that the coherent structures do not always display an axisymmetric character as seen in figure 6*b*, but are positioned randomly with respect to one another across the jet centreline.

Three-dimensional features of the shear layer structure were captured by orienting the laser sheet to illuminate the diametral plane of the jet. The photographs in figure 7 were taken at streamwise positions of $x/D = 2.5$, 3.75, 5 and 7.5; the axisymmetric

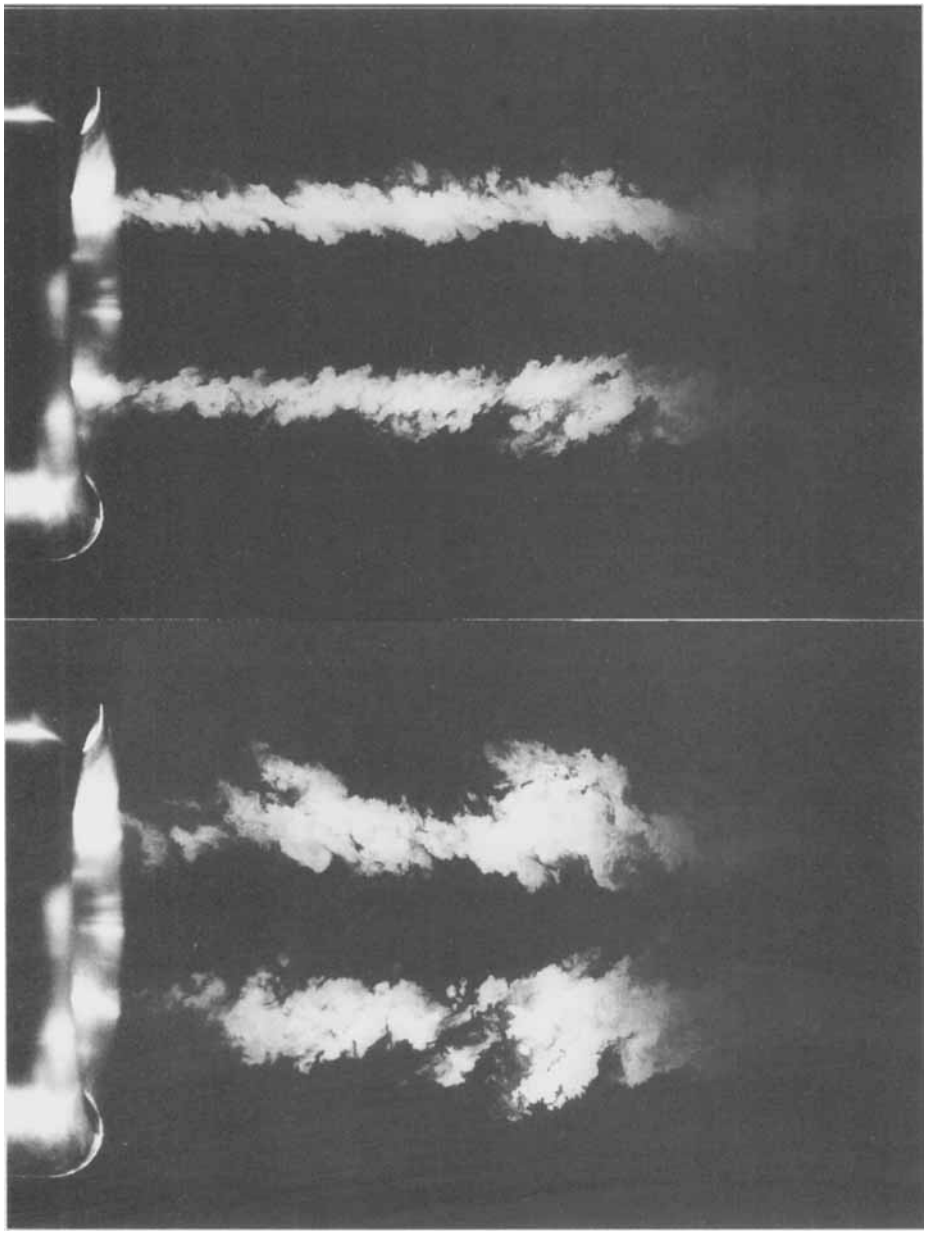

FIGURE 6. Instantaneous images of jet centreplane: (*a*) free jet, and (*b*) jet with counterflow.

mixing region appears slightly oblong owing to the off-axis alignment of the camera with the principal flow direction. The images in figure 7(*a*) are quite representative of those taken in the free jet, indicating very little structure at the convective Mach number of 0.85; structures observed in the diametral plane are typically associated with concentrated streamwise vorticity in the shear layer. The mixed fluid at the farthest downstream location ($x/D = 7.5$) indicates the existence of a finite potential core at that position which agrees with the axial distribution shown in figure 4, where the core is seen to end at $x/D \approx 10$. Although small lobes of fluid could be observed around the

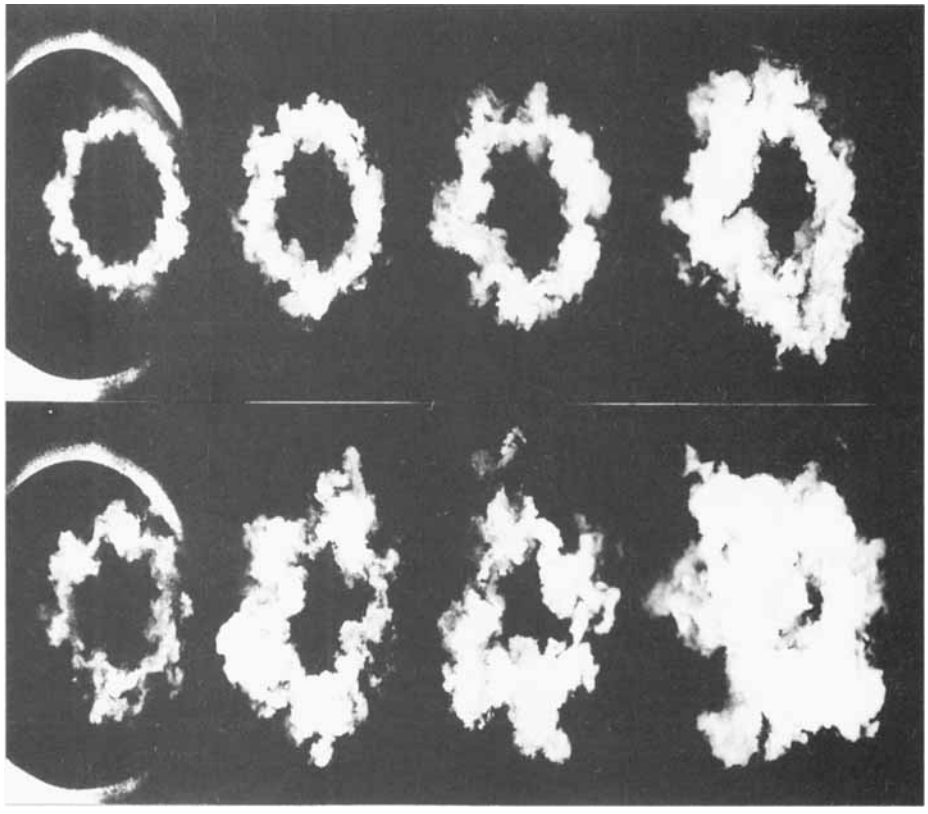

FIGURE 7. Instantaneous images of the jet diametral plane at $x/D = 2.5$, 3.75, 5 and 7.5: (*a*) free jet, and (*b*) jet with counterflow.

jet periphery at this convective Mach number it was difficult to quantify their number with any certainty.

In contrast to the images in figure 7(*a*), the mixing layer clearly shows the presence of large structure when the counterflow is set up within the collar region of the jet (figure 7*b*). Distinct lobes consistently numbering between 5 and 7 were observed within the mixing layer and undoubtedly contribute to the rapid diffusion of the jet. It was observed that the structures were non-stationary, but positioned randomly in space and time about the jet circumference. Stationary streamwise-aligned vortical structures have been observed in underexpanded and ideally expanded jets (Zapryagaev & Solotchin 1988; Novopashin & Perepelkin 1989; Krothapalli, Buzyna & Lourenco 1991; King, Krothapalli & Strykowski 1994), but in these flows the origin of the structure could be traced to minute imperfections residing in the surface of the splitter plate or nozzle near separation. Consequently, the highly three-dimensional nature of the mixing layer observed in figure 7(*b*) is believed to be the result of an inherent instability of the compressible shear layers due to counterflow. One final observation which was made from the instantaneous diametral images is that the mixing region does not precess about the jet axis. In other words, the enhanced diffusion of the jet is due to the presence of highly amplified two- and three-dimensional disturbances and not the tendency of the jet to randomly attach to the collar, giving the artificial appearance of diffusion as is the case in the so-called flip-flop jet (Raman, Hailye & Rice 1992).

Before we take up a discussion of the instability characteristics of compressible countercurrent shear layers in §6, we continue our discussion of the shear layer development with and without counterflow by presenting detailed growth rate measurements in the next section.

5. Growth rate measurements

A quantitative measure of shear layer growth rates was made using a total head probe mounted on a three-dimensional traversing system. Since stationary streamwise vortical structures have been observed in ideally expanded jets (King *et al.* 1994), it was first necessary to perform azimuthal pressure surveys in the shear layer to determine whether minute imperfections in the nozzle may be responsible for variations in the circumferential direction, which might have deterministic effects on the growth rate measurements; the azimuthal surveys were also used to align the probe with the true jet axis. Data were obtained by traversing the probe in 10° increments around the entire jet periphery (see §3.2 for a discussion of the probe characteristics). All measurements were recorded as absolute local stagnation pressures p_t assuming standard isentropic relations in the subsonic regions and by applying Rayleigh's Pitot formula when a normal shock existed upstream of the probe; local static pressures were assumed to be invariant across the jet at any streamwise station. Growth rate measurements were computed using both p_t and Pitot pressures. This was done to evaluate the impact of cross-stream static pressure variations on growth rate measurements. Growth rates evaluated by both techniques yield virtually identical results; error analysis of the measurements will be presented below.

Profiles obtained at an axial location of $x/D = 3.75$ and two different radial positions are shown in figure 8. Small pressure undulations having peak-to-peak amplitudes less than 5 p.s.i. can be observed around the jet periphery. These variations could be reproduced precisely between runs taken over a period of several days, and are not the consequence of data sampling time or experimental uncertainty. By rotating the nozzle it was further observed that these perturbations originated at the nozzle itself in a fashion first proposed by Novopashin & Perepelkin (1989). In the neighbourhood of $\theta = 0°$ a rather large excursion in the pressure can be identified having a magnitude of roughly 20 p.s.i. Profiles taken at the other radial location as well as at different streamwise positions confirmed the presence of the distinct w-shaped undulation commonly associated with a pair of counter-rotating streamwise structures in the shear layer (Arnette, Samimy & Elliot 1993).

Encouraged by the apparent connection between the shear layer response and the nozzle itself we removed the nozzle and carefully measured its inner surface on a lathe with a 2.5 μm resolution surface micrometer. Small irregularities having peak-to-peak heights less than approximately 15 μm were observed around the nozzle lip which can be expected under normal machining operations. However, near the location where the large pressure excursion was measured at $\theta = 0°$ a flat spot was identified having a height of 60 μm. This protuberance – barely noticeable to the touch – clearly has an impact on the shear layer development in the neighbourhood of $\theta = 0°$ and demonstrates how influential even small imperfections in the nozzle boundary layer can be in determining the three-dimensional flow evolution. To minimize the impact of the perturbation on the evaluation of the growth rates, all measurements presented below were made at an azimuthal position of 180°.

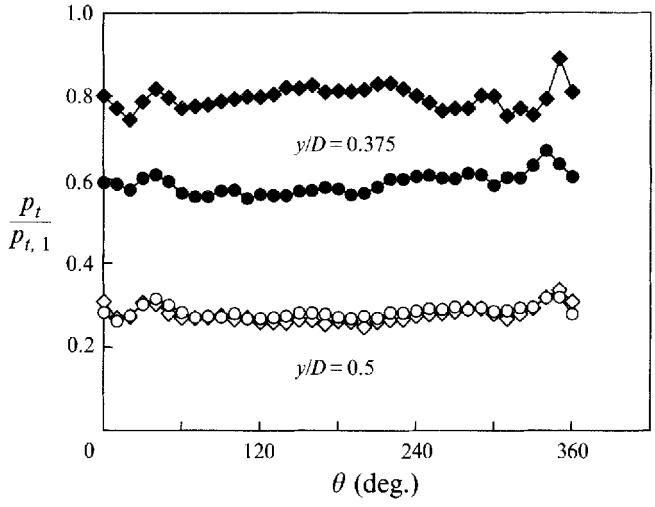

FIGURE 8. Azimuthal mean pressure profiles taken at $x/D = 3.75$. Diamond symbols indicate the free jet and circles show the jet with counterflow.

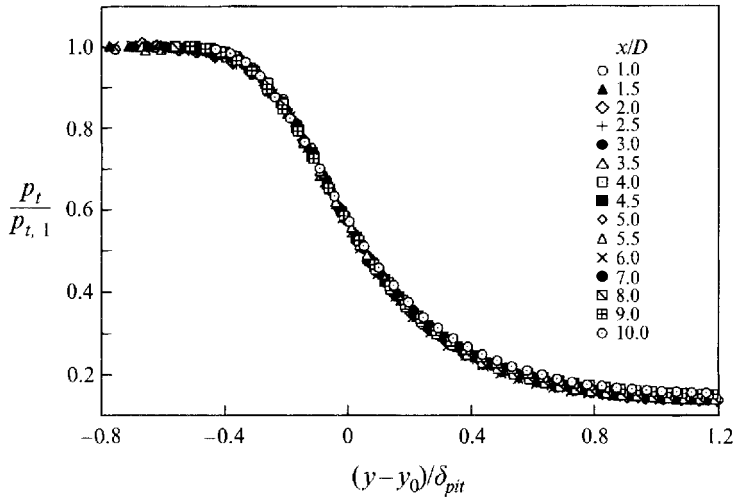

FIGURE 9. Cross-stream total pressure profiles in the free jet.

5.1. *Pitot thickness measurements*

The spatial growth rate of the mixing layer was defined using the Pitot thickness as employed by Papamoschou & Roshko (1988), where δ_{pit} is the distance between the transverse locations where the total pressure is 5% and 95% of the differential total pressure across the layer. The pressure profiles were normalized by the centreline stagnation pressure in the jet $p_{t,1}$ and the transverse coordinate was displaced using the location y_0 where the total pressure was equal to the average of the free-stream values and then normalized using the local Pitot pressure δ_{pit}. Profiles obtained in the free jet at $T_{t,1} = 300$ K and for streamwise positions from $x/D = 1$ to 10 are presented in figure 9. The data indicate reasonable self-similarity in mean quantities up to $x/D \approx 8$, downstream of which some deviation is observed owing to the merging of the opposing shear layer in this region. Downstream of $x/D \approx 10$ the profiles rapidly diverge in the normalized coordinate space owing to the termination of the potential core as seen in figure 4.

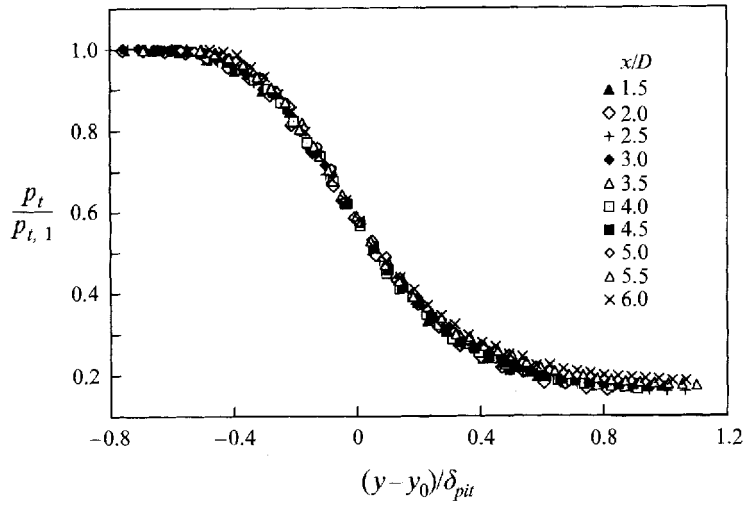

FIGURE 10. Cross-stream total pressure profiles in the jet with counterflow.

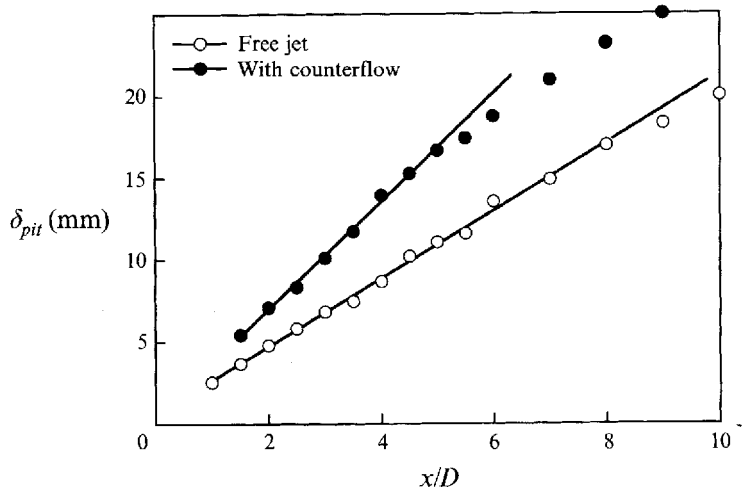

FIGURE 11. Streamwise development of the shear layer thickness in the free jet and the jet with counterflow.

A corresponding series of measurements were made in the shear layers of the counterflowing jet at $r = -0.13$ and $s = 0.55$. The axial Mach number distribution shown in figure 4 indicates that strict self-similarity cannot be expected throughout the potential core region since deceleration occurs between $x/D = 0$ to 2.5; however, a nearly constant-pressure region can be seen from $x/D = 2.5$ to 5 prior to the merging of the shear layers. Notwithstanding this limitation (see additional discussion in §5.2) we measured the spatial development to perform a comparative assessment of growth rates with and without counterflow. The shear layer profiles shown in figure 10 indicate that mean flow self-similarity is achieved at least in the domain from $x/D \approx 2$ to 5 and approximately so slightly upstream and downstream of this region; again rapid divergence can be observed after the shear layers merge near $x/D = 5.0$.

The local shear layer thickness δ_{pit} was obtained from the Pitot profiles and recorded as a function of streamwise distance in figure 11. Linear growth in δ_{pit} is clearly seen

in both shear layers, but the linear regime extends much farther downstream in the free jet since the lower growth rate delays the shear layer merging process. The distinctive feature of the data is seen in the increased spatial growth rate, defined as $d\delta_{pit}/dx$, by roughly 60% when counterflow is applied. A least-squares fit to the free jet data (using the first 13 points) and to the counterflowing jet data (using the first 8 points) provides growth rates of $d\delta_{pit}/dx$ equal to 0.074 and 0.117, respectively. The growth rate in the shear layer without counterflow agrees quite well with published values obtained at comparable convective Mach numbers (e.g. Papamoschou & Roshko 1988; Clemens & Mungal 1992).

To rigorously demonstrate flow self-similarity it is necessary to consider turbulent quantities in addition to the mean shear layer properties provided by the Pitot profiles. Some insight into the fluctuating field can be obtained from the disturbance pressure distributions discussed in §4. In a region of self-similarity turbulence quantities should display a constant peak value, which is clearly not the case for the maximum fluctuating pressure shown in figure 5. The disturbance pressure p' in the shear layer without counterflow varies between 2% and 6% of the stagnation pressure over the streamwise distance of $x/D \approx 1$–8 where the mean flow quantities exhibit self-similarity. The variation in p' is somewhat surprising given that the Reynolds number based on ΔU, δ_{pit} and average mixing layer properties is so high, varying between 1.5×10^5 and 10^6; Goebel & Dutton (1991) suggest that a Reynolds number of approximately 1.25×10^5 should be sufficient to achieve self-similarity in the Reynolds stress distribution for compressible flow. By contrast, the p' distribution in the counterflowing jet ($r = -0.13$) displays a nearly constant value in the region of x/D between 2.5 and 5, where the Reynolds number varies between 4.7×10^5 and 10^6. If we were to demand a Reynolds number of at least 4.7×10^5 for self-similarity of turbulence quantities in the shear layer without counterflow, we then would observe a significantly smaller variation in p' from 5% to 6% over the range of $4 \leqslant x/D \leqslant 8$. Given the fact that the finite size of the fluctuating pressure probe will tend to underestimate p' close to the nozzle where δ_{pit} is small, we can conclude that perhaps a Reynolds number of 4.7×10^5 is too restrictive but probably representative for the flow we have examined. Despite our inability to define the self-similar region more precisely, it is nonetheless important to emphasize the principal finding that spatial growth rates can be increased by 60% when counterflow is applied over a finite region in the jet near field.

5.2. *Visual growth rate measurements*

All measurements presented thus far have considered the response of the compressible shear layer to a fixed level of counterflow corresponding to a velocity ratio of -0.13 and a density ratio of 0.55. To elucidate the relationship between shear layer growth rate and velocity ratio a visualization study was conducted in the cold supersonic jet ($T_{t,1} = 300$ K) using the product formation method described in §3.2. This approach served both as an independent verification of the Pitot thickness measurements and as a relatively expedient method for estimating growth rates. Visual estimates of the shear layer thickness δ_{vis} were made over a streamwise distance roughly equivalent to that used to compute the growth rates from the Pitot measurements. Planar images of the time-integrated behaviour of the mixing layer were obtained by exposing the film to 20 superimposed images over a period of approximately 2 s.

Photographs obtained in the free jet ($r = 0$) and at the extreme velocity ratio studied ($r = -0.16$) are shown in figure 12.† The images extend over a streamwise distance

† A slightly lower velocity ratio of -0.16 was achieved during this portion of the study by a moderate reduction in the pressure losses of the vacuum system used to create counterflow.

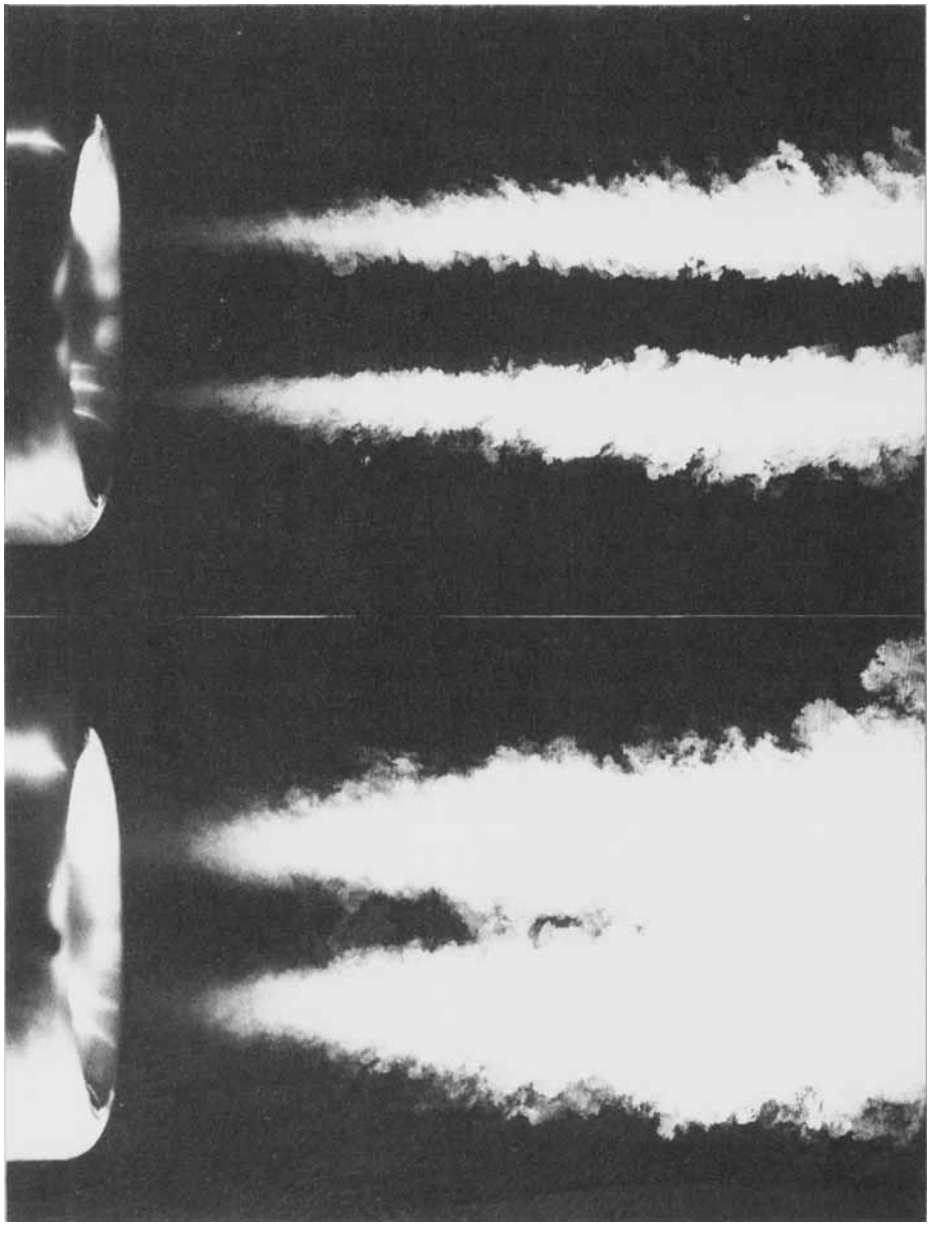

FIGURE 12. Time-integrated exposures of the jet centreplane: (*a*) free jet, (*b*) jet with counterflow.

between 2.5 and 7 diameters and unambiguously show the rapid diffusion of the shear layer caused by counterflow. Visual growth rates $d\delta_{vis}/dx$ obtained from the images were 0.10 and 0.16 for the free jet and the counterflowing jet, respectively. Papamoschou & Roshko (1988) suggest that visual growth rates based on schlieren images should be approximately 20% higher than those from Pitot measurements which does not entirely account for the 35% difference in the two approaches, although a strict comparison between δ_{vis} obtained from schlieren and planar laser scattering has not been performed to our knowledge. However, the relative comparison

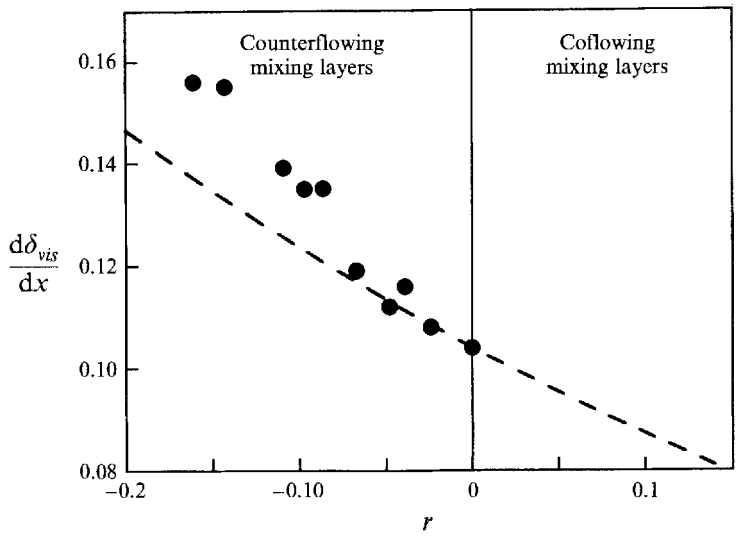

FIGURE 13. The symbols indicate the growth rates obtained in the jet with counterflow. The dashed curve represents the theoretical growth rates predicted by equation (1).

between the free jet and counterflowing jet using planar imaging is quite good and confirms the 60% increase in spreading rate found using $d\delta_{pit}/dx$.

Planar images of the shear layer were obtained over a range of secondary velocities to estimate the dependence of $d\delta_{vis}/dx$ on velocity ratio; a summary of those results is provided in figure 13 for the flow conditions at a density ratio of $s = 0.55$. The velocity ratio is divided into half-planes where values of $r < 0$ indicate the class of countercurrent mixing layers and values of $r > 0$ denote coflowing layers. The experimental results from the present study lie in the negative half-plane and display a nearly linear relationship between velocity ratio and growth rate. To compare the results obtained for countercurrent mixing layers with those of coflowing layers, we assume that the compressible growth rate can be expressed in the form

$$\frac{d\delta_{vis}}{dx} = \frac{C_1 C_2 (1-r)(1+s^{1/2})}{(1+rs^{1/2})}, \tag{1}$$

from Papamoschou & Roshko (1988), where the constant C_1 depends on the convective Mach number and C_2 depends on the technique used to evaluate the growth rate (e.g. visual thickness versus Pitot thickness). We determined the product $C_1 C_2 = 0.059$ in our experiments by requiring agreement between the negative and positive half-planes at $r = 0$, where the growth rate was measured as $d\delta_{vis}/dx = 0.10$ at a density ratio of $s = 0.55$. The product $C_1 C_2$ agrees reasonably well with values in the literature if we take C_1 as the normalized compressible growth rate of 0.33, which is essentially constant for convective Mach numbers greater than 0.8 (e.g. see figure 4 of Clemens & Mungal 1992), and multiply it by the value of $C_2 = 0.17$, which correlates the incompressible data of visual thicknesses from schlieren images, obtaining a value of $C_1 C_2 = 0.055$.

The dashed line in figure 13 shows the predicted compressible growth rates from equation (1) over positive and negative velocity ratios for conditions at $s = 0.55$. The experimental growth rates appear to follow the model at moderate levels of

counterflow, but clearly deviate from the theoretical curve in the neighbourhood of $r = -0.07$, leading to growth rates in considerable excess of the predicted values. To begin to understand the physical origin of the transition observed in figure 13 at negative velocity ratios we must first reconsider the nature of the countercurrent mixing layer which has been established in the near field of the jet. In the absence of direct measurements of U_2 within the collar, we assumed a uniform velocity distribution in the secondary stream in the jet exit plane ($x = 0$) and obtained estimates of U_2 by monitoring the secondary mass flow; the velocity ratio, density ratio and convective Mach number were corresponding defined at $x = 0$. But owing to an adverse pressure gradient within the collar, the primary stream decelerates resulting in a streamwise variation in these quantities over the region in which we obtain spatial growth rate measurements.

To elaborate this point we return to the counterflow conditions of $r = -0.13$ examined in detail above. In the jet exit plane, where r is defined, the primary and secondary velocities are 520 m s^{-1} and -65 m s^{-1}, respectively, at a stagnation temperature of $T_{t,1} = 300$ K. After the flow decelerates in the collar region ($0 \leqslant x \leqslant L$) the local primary-stream velocity has been reduced to 495 m s^{-1} and the counterflow velocity is essentially zero; these conditions are maintained up to the termination of the potential core at $x/D = 5$. From the local quantities the flow conditions were computed in the jet exit plane as $r = -0.13$, $s = 0.55$ and $M_c = 0.96$, and downstream in the constant-pressure potential core ($L/D < x/D \leqslant 5$) as $r \approx 0$, $s = 0.58$, and $M_c = 0.82$.

We now consider how these spatial variations may impact on our evaluation of the compressible growth rates obtained by measurement of either δ_{pit} or δ_{vis}. Corroborating the work of Papamoschou & Roshko (1988), many investigators have observed that the shear layer growth rate is insensitive to the *level* of compressibility if the convective Mach numbers is greater than approximately 0.8. This implies that variations in compressibility, due to changes in M_c along the potential core, will have little impact on the dynamics of the mixing layer since M_c is everywhere greater than 0.8. Consequently, we examined the sensitivity of $\mathrm{d}\delta/\mathrm{d}x$ to variations in s and r to evaluate the leading parameter responsible for the elevated growth rates seen in figure 13. From (1) we estimate that the 5% increase in density ratio from $x = 0$ to $x = L$ will result in an increase in spatial growth rate of less than 1.5%, which clearly cannot account for the experimental observations. Therefore, we believe that the trend reported in figure 13 is uniquely due to variations in velocity ratio.

The rather large gradient in velocity ratio within the collar region must also be considered as a potential source of uncertainty in the measurements. For instance, over the spatial domain where Pitot measurements were made, we expect some variation in velocity ratio up to $x \approx L$. Therefore, extending the linear fit to the data upstream of $x/D \approx 2.5$ in figure 11 is not entirely justified even though the inclusion of the first two data points does not appear to affect the value of $\mathrm{d}\delta_{pit}/\mathrm{d}x$. But the following question remains: since the growth rate measurements are based on the velocity field downstream of the collar where counterflow does not exist, how are we justified in claiming the results are indicative of a countercurrent mixing layer? A definitive answer to this question probably cannot be made without creating a truly self-similar countercurrent plane mixing layer; however, the fact remains that counterflow applied in the jet near field does have a substantial impact on the shear layer evolution downstream. Consequently, we believe the measurements capture the essential physics of the countercurrent mixing layer through their imprint on the spatially developing flow downstream of the collar exit. Despite this limitation, the measurements in figure

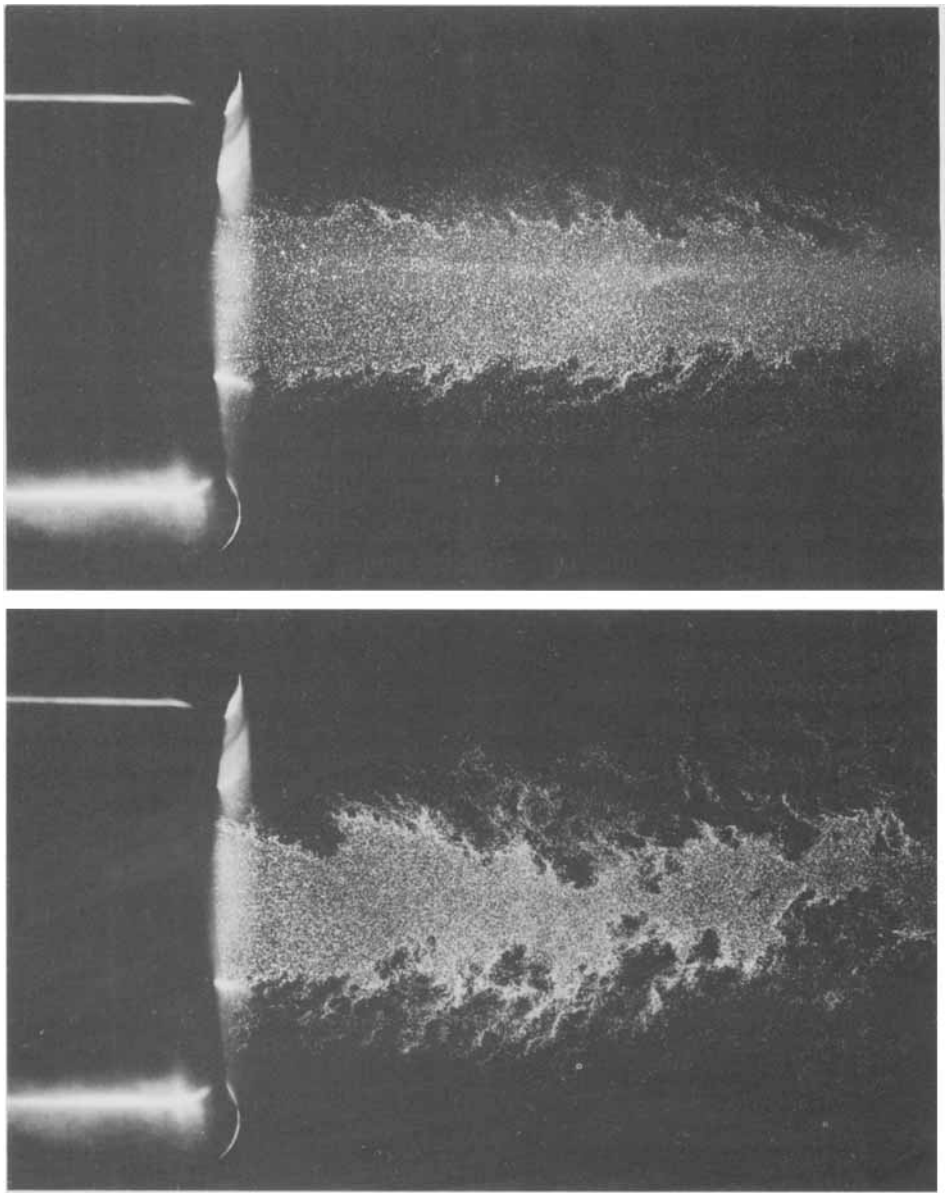

FIGURE 14. Instantaneous images of jet centreplane: (*a*) free jet, and (*b*) jet with counterflow.

13 clearly indicate that shear layer growth rates can be significantly increased in the presence of counterflow, which is important from an engineering perspective owing to the finite spatial domain over which the counterflow was applied.

5.3. *Effects of convective Mach number and density ratio*

By normalizing shear layer growth rates measured in high-speed shear layers by those of incompressible layers taken at similar values of r and s, Papamoschou & Roshko (1988) isolated the independent role of compressibility on the flow evolution. The shape of the normalized growth rate curve (figure 16 of their paper) indicates that compressibility first becomes important at convective Mach numbers above 0.3 and

continues to affect the flow development up to a convective Mach number of approximately 0.8, above which the normalized growth rate is constant. In the range of $M_c > 0.8$ compressibility reduces growth rates to a level roughly $\frac{1}{3}$ of that expected in an incompressible layer at similar velocity and density ratios. Although this indicates the importance of compressibility on the flow development, it also implies that the shear layer dynamics will no longer depend on M_c in this range; in other words, convective Mach number invariance has been reached.

Since our measurements were made near the threshold convective Mach number of 0.8 we felt it would be wise to extend the study of the countercurrent mixing layer to higher convective Mach numbers. This was accomplished by heating the primary flow to a stagnation temperature of $T_{t,1} = 715$ K by activating the in-line electrical tank heaters discussed in §3. At the elevated temperature, the free jet shear layer operated at a convective Mach number of 1.06 and a density ratio of 1.32; the specific heat ratio across the mixing layer γ_2/γ_1 varied by less than 0.5% between the studies conducted at different stagnation temperatures. The counterflowing conditions which were examined correspond to a velocity ratio of -0.07, at a density ratio 1.32, and a convective Mach number of 1.14, as determined in the exit plane at $x = 0$. Owing to flow deceleration in the collar region these quantities achieved the values of $s = 1.39$ and $M_c = 1.01$ in the constant-pressure potential core region formed downstream of the collar.

A qualitative examination of the mixing region was undertaken by seeding the primary stream with fine aluminium oxide particles as described in §3.2. Photographs taken of the axial centreplane of the jet exposed for a duration of 11 ns are shown in figure 14 with and without counterflow; the images extend from approximately 2.5 to 8 diameters downstream of the jet exit. The free jet photograph in figure 14(*a*) illustrates the undisturbed potential core of the flow and the absence of significant diffusion of the shear layers in the exposed region. Since the Stokes number of the aluminium oxide particles is small (see §3.2), suggesting that the particles will follow the flow, we do not expect illumination of the entrained secondary-stream fluid in these images. As shown in figure 14(*b*), we do observe significant excursions of the unmarked fluid into the core region of the jet when counterflow is applied. The photograph of figure 14(*b*) provides an indication of the violent nature of the disturbances in the shear layer with counterflow as well as their scale compared to the free jet shear layer shown in figure 14(*a*).

Images of the jet cross-section were obtained at $x/D = 3.75$ using light scattering from the aluminium oxide particles and are shown in figure 15. The particles seeding the free jet (figure 15*a*) have experienced negligible radial diffusion in comparison to the jet with counterflow ($r = -0.07$). Many of the photographs taken in the counterflowing jet display a radial expulsion of core fluid as seen in the lower right corner of figure 15(*b*); the clarity of the radially directed flow is less distinct at other azimuthal positions owing to the finite depth of field of the lens system used to capture the images. This behaviour implies the presence of a strong streamwise vorticity component associated with the large structure in the shear layer, and is qualitatively similar to the so-call side jets observed in self-excited and highly forced incompressible jets by Monkewitz *et al.* (1989) and Russ, Strykowski & Pfender (1994). A close examination of figure 15(*b*) reveals approximately five locations where we presume there is significant radial outflow, a number which is consistent with the condensation image of figure 7(*b*) at $x/D = 3.75$ where nominally five lobes were identified around the jet perimeter.

To quantify the enhanced radial diffusion suggested by the laser sheet images,

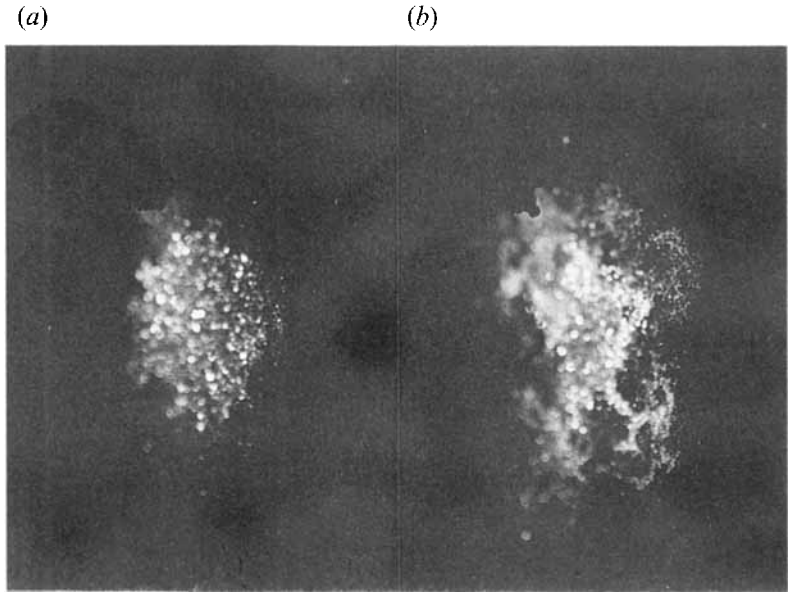

FIGURE 15. Instantaneous images of the jet diametral plane at $x/D = 3.75$: (*a*) free jet, and (*b*) jet with counterflow.

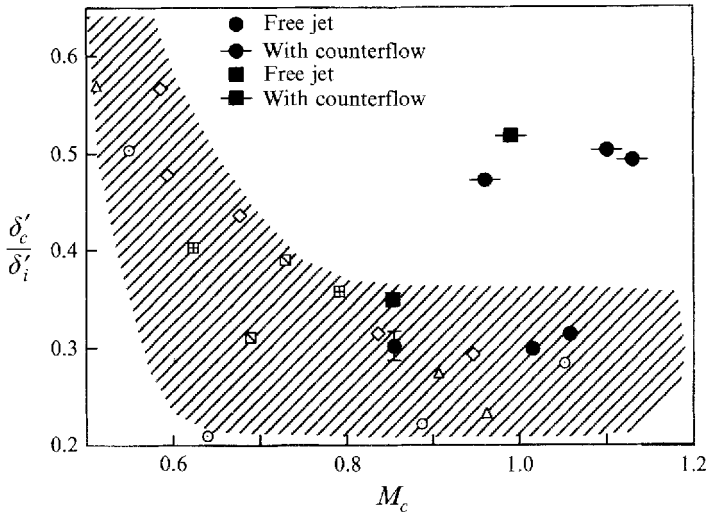

FIGURE 16. Normalized growth rates obtained in the free jet and the jet with counterflow. Solid circles and squares indicate data obtained using Pitot probes and visual measurements, respectively.

detailed Pitot probe surveys were conducted following the approach outlined in §5. Radial profiles having spatial resolution comparable to those presented in figures 9 and 10 were obtained over a streamwise distance corresponding to the potential core region of the jet. Least-squares fits to the data were used to estimate the growth rates and are summarized in figure 16 for data taken over the full range of stagnation temperatures examined in this study. Also included on the figure are the visual growth rates made from the condensation photographs described in §5.2. The quantity δ_c' corresponds to the compressible growth rates determined experimentally either by visual means ($\delta_c' =$

Method	$T_{t,1}$ (K)	M_c	s	r_{min}	$\mathrm{d}\delta_c/\mathrm{d}_x$
Pitot	300	0.96	0.55	−0.13	0.117
Pitot	540	1.10	1.00	−0.10	0.143
Pitot	680	1.13	1.26	−0.07	0.149
Visual	300	0.99	0.55	−0.16	0.156

TABLE 1. Growth rate measurements of the countercurrent shear layer

$\mathrm{d}\delta_{vis}/\mathrm{d}x$) or by Pitot surveys ($\delta_c' = \mathrm{d}\delta_{pit}/\mathrm{d}x$). The compressible growth rates were normalized by δ_i' which is the growth rate predicted by the incompressible model given by Papamoschou & Roshko (1988) as

$$\delta_i' = \frac{C_2(1-r)(1+s^{1/2})}{(1+rs^{1/2})}, \tag{2}$$

where the empirical constant C_2 can be taken to be 0.14 and 0.17 when normalizing growth rates based on Pitot and visual measurements, respectively.

The hatched region in figure 16 indicates a rather broad scatter in experimental results taken from the literature. Measurement uncertainty, when reported, does not account for all of the discrepancy, so it is likely that a combination of reasons may be responsible for the large measurement bandwidth, including data taken outside a region of self-similarity (M. Samimy 1993, personal communication) and differences in initial conditions (Clemens & Mungal 1992). Growth rate estimates from the present study without counterflow are seen to fall well within the reported uncertainty. An nth-order uncertainty analysis (Moffett 1982) was performed for the data taken at $T_{t,1}$ = 300 K without counterflow ($M_c = 0.86; \delta_c'/\delta_i' = 0.302$) to obtain a representative estimate of the uncertainties in growth rate. Included in the analysis, in addition to instrument imprecision, were uncertainties due to probe displacement effects within the layer, errors from the least-squares fitting of the data, as well as uncertainties in computing δ_i' due to variations in r and s. Conservative estimates of these quantities provided a total uncertainty of less than 4% with a 95% confidence as indicated by the vertical error bar in figure 16.

Normalized growth rates are presented in figure 16 for the visual measurements obtained at $T_{t,1}$ = 300 K and for detailed Pitot surveys conducted at temperatures of $T_{t,1}$ = 300, 540 and 680 K. (It was not possible to hold the stagnation temperature to within 0.5% at a nominal value of 715 K over the relatively long time period necessary to collect the pressure profiles, consequently an upper temperature to 680 K was used during this study.) For clarity, only data points corresponding to the minimum velocity ratio at each stagnation temperature are presented; the growth rates are summarized in table 1.

For purposes of comparison, the compressible growth rate δ_c' in figure 16 was normalized by the incompressible value δ_i' taken at s from the table and $r = 0$. This normalization was chosen to account for the observation that $U_2 \approx 0$ in the region where the growth rate measurements were made, and also because there is some question regarding the appropriateness of the incompressible model given by equation (2) when applied at negative velocity ratios. Using this normalization, the growth rates with counterflow are consistently 60% greater than the corresponding values in the free jet at all density ratios examined. If, on the other hand, we assume that the density and velocity ratios measured in the jet exit plane are representative of the shear layer dynamics downstream of the collar and we normalize by δ_i' evaluated at r and s from

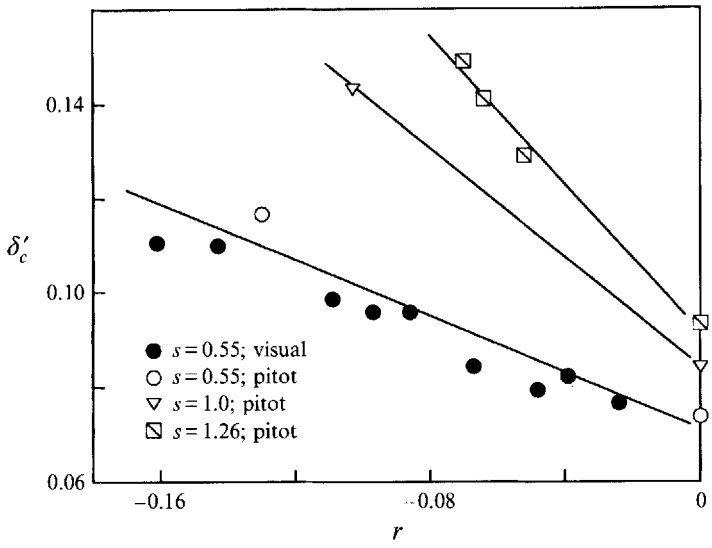

FIGURE 17. Dependence of compressible growth rate on velocity ratio.

the table, the values of δ_c'/δ_i' are still between 30% and 40% greater than those predicted from the existing literature at all convective Mach numbers studied.

The inability to collapse the compressible growth rate data using the incompressible model given by (2) demands further inquiry. First, it is necessary to consider the validity of the relationship given by $\delta_i' = \delta_i'(r, s)$ which is based on physical arguments for a purely convectively unstable system which may not be relevant at negative velocity ratios. This issue will be addressed by studying the spatio-temporal theory of compressible countercurrent shear layers in §6. We can, however, isolate the functional dependence of δ_c' on velocity and density ratios if we assume that changes in compressibility will only play a minor role in the shear layer dynamics. This seems reasonable since the convective Mach number is greater than 0.8 for all shear layers examined during this study. We can identify the relationship $\delta_c' = f(r, s)$ by presenting all growth rate measurements in the velocity ratio space as shown in figure 17. To accommodate both Pitot and visual estimates of δ_c' we corrected the values of $\mathrm{d}\delta_{vis}/\mathrm{d}x$, taken from figure 13, by the constant C_2 necessary to force agreement between the visual and Pitot measurements at $r = 0$. The dependence of δ_c' on r obtained from the two independent studies at $s = 0.55$ is in good agreement over the range of velocity ratios examined.

The curves in figure 17 show that the compressible growth rate can be increased up to approximately 60% at all density ratios, in agreement with the minimum r-values presented in figure 16. However, the magnitude of the counterflow necessary to achieve a particular growth rate is a strong function of the density ratio. The data clearly indicate that less counterflow is required to reach similar levels in δ_c' when the density of the primary stream is less than the density of the secondary stream, i.e. when s is greater than unity. The function $f(r, s)$ can be estimated using the following heuristic arguments. First, we know that the effect of density ratio on the compressible growth rate can be eliminated at $r = 0$ by employing the scaling factor of $1 + s^{1/2}$ which is proportional to the incompressible growth rate at zero velocity ratio (see equation (2)). This scaling effectively unifies values of δ_c' at $r = 0$ for the data in figure 17, but not for negative velocity ratios. The data can be described universally over the present parameter space through the observation that the growth rate for $r < 0$ is directly

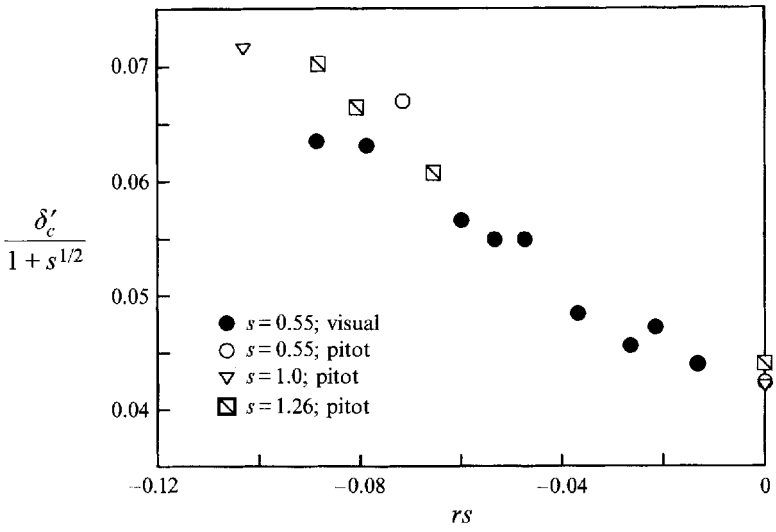

FIGURE 18. Dependence of normalized compressible growth rate on mass flux ratio.

proportional to the magnitude of r and s. This implies that the scaling parameter is the mass flux ratio rs which together with the ordinate of $\delta_c'/(1+s^{1/2})$ is seen to collapse the data reasonably well in figure 18. The reason for this scaling is unclear but must be related to the unique stability of the countercurrent mixing layer. This question motivated an examination of the spatio-temporal theory of compressible shear layers for negative velocity ratios which is the topic of the next section.

6. Stability of compressible countercurrent shear layers

The connection between the local flow properties of absolute and convective instability and the global flow response has been discussed in detail by Huerre & Monkewitz (1985, 1990) and Chomaz *et al.* (1988), among others. These studies conclude that spatial stability theory appropriately describes the flow evolution if local conditions are dominated by a convective instability, but that temporal theory is required to accurately describe the development if a sufficiently large domain of the flow is absolutely unstable. Many investigations have examined the convective–absolute transition over a wide range of flow conditions including wakes (Koch 1985; Monkewitz & Nguyen 1987; Hannemann & Oertel 1989), jets (Monkewitz & Sohn 1988; Jendoubi & Strykowski 1994), and mixing layers (Huerre & Monkewitz 1985; Pavithran & Redekopp 1989; Jackson & Grosch 1990; also for confined mixing layers see Peroomian & Kelly 1994).

In the present context we refer to the closely related work of Pavathran & Redekopp (1989), Jackson & Grosch (1990), and Jendoubi & Strykowski (1994), where the neutral boundary separating absolute and convective instability has been identified in plane and axisymmetric mixing layers. These authors found that subsonic mixing layers become increasingly unstable by reductions in either velocity ratio or convective Mach number or increases in density ratio. But it was observed that absolute instability can only be supported in mixing layers at negative velocity ratios, i.e. for $U_2 < 0$. Furthermore, the magnitude of the counterflow necessary to reach the neutral boundary was found to be quite excessive, in particular if the trends at subsonic Mach numbers were indicative of those extended to supersonic flow conditions. The aim of

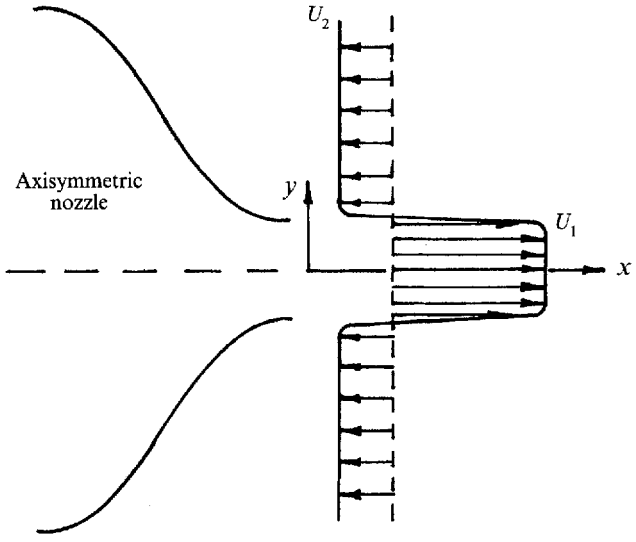

FIGURE 19. Axisymmetric counterflowing jet.

the present analysis was to extend the calculations to convective Mach numbers greater than unity to evaluate whether absolute instability could be responsible for the global flow development in the supersonic jet examined in the experimental portion of this study. An overview of the analysis is presented below and the reader is referred the work of Jendoubi & Strykowski (1994) for a more detailed discussion.

The geometric configuration of the jet to be investigated is shown in figure 19. The axial, radial, and angular directions of the flow are denoted by x, y, and ϕ, respectively. Fluid of centreline static temperature T_1 and velocity U_1 is surrounded by ambient fluid having a temperature and velocity given by T_2 and U_2, respectively, where the ambient flow direction can be taken to be either coflowing or counterflowing to the jet fluid; both streams are considered to be inviscid and the ambient fluid extends to infinity in the radial direction. The mean flow is assumed to be laminar and locally parallel to the jet axial direction, and the axisymmetric streamwise velocity distribution is taken to have the following cross-stream dependence:

$$U(y) = \frac{1+r}{2} + \frac{1-r}{2}\tanh\left[\frac{D}{8\theta}\left(\frac{1}{y} - y\right)\right], \tag{3}$$

where D is the jet diameter and θ is the momentum thickness of the shear layer; the temperature distribution is taken to satisfy the Busemann–Crocco relation (Schlichting 1978).

The stability of the axisymmetric shear layer is studied by introducing a perturbation of the form

$$q' = q'(x, y, \phi, t) = q(y)\,\mathrm{e}^{\mathrm{i}(\alpha x + m\phi - \omega t)}, \tag{4}$$

which assumes that the fluid motion can be divided into a mean component and disturbed motion, where q' represents any fluctuating quantity. The wavenumber α and frequency ω are complex quantities allowing disturbance growth in space and time, and m is the azimuthal mode number; $m = 0$ represents axisymmetric waves and $m \neq 0$ indicates helical modes. Following an analysis originally proposed by Michalke (1971), a nonlinear differential equation for the disturbances is solved using a shooting method. For a prescribed profile shape defined by a choice of $D/\theta, s, r$, and M_c, as well

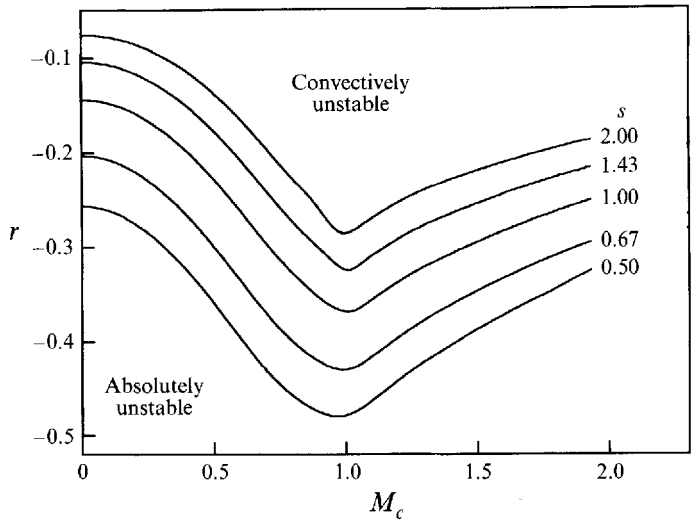

FIGURE 20. Absolute–convective stability boundary for axisymmetric disturbances.

as a selection of wavenumber α and mode number m, integration yields the eigenvalue ω satisfying the disturbance equations and boundary conditions. Many investigations (Briggs 1964; Akhierzer & Polovin 1971; Bers 1983; Huerre & Monkewitz 1985) developed criteria for identifying whether wave growth in an unstable system would evolve locally or the wave would be convected away from its origin during amplification. In particular, it must be determined whether the wave having zero group velocity is amplified or damped in time, the former corresponding to an absolute instability and the latter to convective instability. (The zero group velocity wave must also satisfy the pinching requirement; see Bers 1983.)

The neutral boundary separating regions of convective and absolute instability was identified for the velocity profile defined by (3) in a parameter space involving r, s, and M_c. The neutral boundary for axisymmetric waves ($m = 0$) in the (r, M_c)-plane is shown in figure 20 at several values of s. The region above each s-curve corresponds to convective instability and the region below to absolute instability. All stability boundaries display a monotonically decreasing stability with increasing density ratio. In other words, for fixed coordinates of r and M_c the flow tends toward absolute instability as the primary density is reduced relative to the secondary stream, e.g. as the jet temperature is increased. It can also be observed that absolutely unstable flow is only possible in the presence of counterflow. The stability boundaries at subsonic convective Mach numbers are in close agreement with those of Huerre & Monkewitz (1985) and Pavithran & Redekopp (1989) indicating that absolute instability can be achieved in low-speed flows with very modest levels of counterflow, but that significant backflow is required as the convective Mach number is increased.

Perhaps the most interesting result of figure 20 is the dependence of the convective–absolute boundary on M_c. Independent of density ratio, it can be seen that the stability behaviour is abruptly reversed as the convective Mach number passes from subsonic to supersonic. At fixed values of r and s the flow tends toward absolute instability, and away from convective instability, with increasing convective Mach number in the domain where $M_c > 1$. Hence, the convective Mach number uniquely identifies two distinct flow regimes, a property not displayed by other parameters such as the primary-stream Mach number U_1/a_1 (also see Jackson & Grosch 1990). Furthermore, the trend seen for $M_c > 1$ in figure 20 has not been reported previously

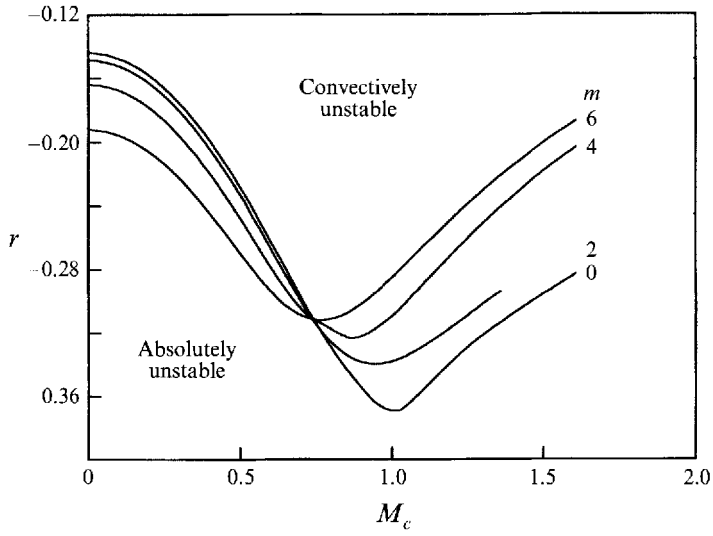

FIGURE 21. Absolute–convective stability boundary of helical disturbances for $s = 1.0$.

in studies where purely spatial or purely temporal theory has been examined such as the work of Gropengiesser (1970), indicating the importance of including wave growth in space and time.

A close examination of the stability curves in figure 20 reveals that considerable counterflow is required to reach absolute instability at the density ratios of the counterflowing jet summarized in table 1. The minimum r-value of -0.13 achieved experimentally at $s = 0.55$ ($M_c = 0.96$) can be compared to a theoretical value on the neutral curve, separating regions of convective and absolute instability, of $r_{cr} = -0.465$. Theoretical values of r_{cr} obtained at density ratios of 1.00 ($M_c = 1.10$) and 1.26 ($M_c = 1.13$) are -0.356 and -0.321, respectively. Although considerably less counterflow is required to reach r_{cr} as the density ratio is increased, the magnitude of the counterflow in the experiments is clearly insufficient to expect the local velocity field to support the absolute instability of two-dimensional disturbances.

The highly three-dimensional character of the counterflowing jet, as indicated by the images of figures 7 and 15, suggests that the stability of two-dimensional waves alone cannot be expected to account for the experimental observations. Sandham & Reynolds (1990) have shown that the most spatially unstable waves in plane mixing layers undergo a transition from two-dimensional to oblique as the convective Mach number is increased above 0.6. Consequently, it can be anticipated that helical waves may become absolutely unstable in the axisymmetric shear layer as M_c is increased. Therefore, we extended the spatio-temporal theory to include azimuthal mode numbers up to $m = 6$; a representative family of stability curves for $s = 1$ is presented in figure 21. The non-monotonic relationship between r_{cr} and M_c is borne out for all mode numbers; however, the minimum r-value occurs at lower convective Mach numbers as m is increased. This leads to a transition at $M_c \approx 0.75$ where helical waves become more unstable than axisymmetric ones. Stability calculations performed at other density ratios indicate that the critical convective Mach number is relatively insensitive to density ratio (e.g. $M_c \approx 0.76$ at $s = 2.0$). Hence, for all convective Mach numbers examined in the experiments we anticipate that the flow will be dominated by three-dimensional disturbances even if the conditions necessary to achieve absolute instability are not satisfied.

A comparison of the stability boundaries from figure 21 reveals a reduction in the magnitude of r_{cr} from 0.356 to 0.265 for modes $m = 0$ and $m = 6$, respectively, at the corresponding experimental conditions from table 1 ($s = 1.0$; $M_c = 1.10$). Although there is a significant reduction in the level of counterflow needed to establish local absolute instability for three-dimensional waves, the theoretical velocity ratios are still significantly lower than the velocity ratios reported experimentally ($r > -0.10$ for $s = 1.0$). However, one of the difficulties of comparing the theoretical and experimental results lies in the fact that the measured velocity ratios are based on estimates of U_2 made in the jet exit plane which may not be entirely representative of the flow conditions within the collar itself. The pressure perturbation profiles obtained in the shear layer (figure 5) together with flow visualization (figures 6 and 14) suggest that the disturbance levels will be quite high in the shear layer of the counterflowing jet. These conditions will give rise to significant cross-stream momentum transport and enhanced entrainment of the secondary stream by the primary jet. Consequently, a large fraction of the mass which enters the collar from the ambient air will be carried away in the primary stream, and the remainder will be drawn into the collar and vacuum system.

Recent measurements reported by Strykowski, Krothapalli & Forliti (1995) in a rectangular jet with counterflow under nearly identical conditions to the present study indicate that flow accelcration within the collar results in a variation in velocity ratio from -0.10 in the jet exit plane to -0.40 within the collar itself. (These measurements were made at $s = 0.55$ and $M_c = 0.94$ using particle image velocimetry in a rectangular jet operating at a primary stream Mach number of 2. This non-intrusive technique was not employed in the present study owing to the severe restriction imposed by the axisymmetry of the collar geometry.) The significant acceleration of the secondary flow suggests that the conditions for local absolute instability may be set up within the collar. Whether a sufficiently large region of the flow can support absolute instability and thereby self-excitation is still an open question. However, the experiments do provide convincing evidence that moderate levels of secondary flow drawn through the vacuum system can result in significant increases in shear layer growth rate. This is particularly important given the theoretical prediction that less counterflow will be required as the primary-stream density is reduced, since this is the case in a high-temperature jet exhaust.

7. Summary and conclusions

A series of experiments were performed in a Mach 2 axisymmetric jet to examine the influence of counterflow on compressible shear layer development. A secondary stream, travelling in the direction opposed to the primary flow, was used to establish negative velocity ratios in the laboratory frame of reference. Growth rates of the compressible shear layer obtained using Pitot surveys and flow visualization indicate that significant shear layer diffusion can be achieved using counterflow. Spatial growth of the shear layer at negative velocity ratios was almost 60% greater than that measured in a coflowing layer at a similar density ratio and convective Mach number. Instantaneous planar light sheet imaging of the flow revealed that distinct three-dimensional structures develop in the shear layer owing to counterflow; fast response pressure transducers were also employed to verify enhanced turbulence levels in the countercurrent shear layer. Heating of the primary flow was used to extend the range of convective Mach numbers studied and to evaluate the influence of density ratio on the flow development. It was observed that spatial growth rates at negative velocity ratios were proportional to the mass flux ratio across the shear layer. The spatio-

temporal stability of the compressible axisymmetric shear layer was examined to identify the neutral curve separating regions of convective and absolute instability in the flow. Contrary to results obtained using spatial theory alone, the spatio-temporal theory indicates that the shear layer becomes increasingly unstable as the convective Mach number is increased for values of M_c greater than unity.

One of the primary motivations for the present study was the development of efficient control schemes for the rapid diffusion of compressible shear layers. The underlying premise of the research was the belief that viable approaches to shear layer control should exploit the inherent instability of the flow thereby eliminating the need for externally driven actuators which would require considerable power consumption – in practice the inherent instability may affect the global flow development through self-excitation. Berman & Ffowcs Williams (1970) described this approach as perhaps the most promising one to tackle the challenging problem of suppressing supersonic jet noise. Encouraged by the success of employing counterflow to enhance subsonic jet diffusion (Strykowski, Krothapalli & Wishart 1993), we extended the concepts to convective Mach numbers where mixing between dissimilar streams is relatively poor. Although the experimental results clearly indicate the important role of counterflow in shear layer diffusion, the connection between the laboratory observations and the underlying theoretical framework remains unclear.

Spatio-temporal theory does indicate that absolute instability can be achieved for both two- and three-dimensional disturbances at supersonic convective Mach numbers at modest negative velocity ratios. However, the experimental results suggest that enhanced shear layer diffusion can be achieved at levels of counterflow significantly less than would be required for absolute instability. This finding, together with the fact that a global bifurcation was not observed at velocity ratios less than zero, suggests that the enhanced diffusion is principally caused by the increased shear of counterflow coupled with the reduced convective velocities expected at negative velocity ratios. Measurements made in compressible plane shear layers (Strykowski *et al.* 1995) suggest that the counterflow within the collar region may be higher than that observed in the jet exit plane. Whether or not these levels are sufficiently high to support absolute instability in the present flow is unknown, but this may explain why the experimentally determined growth rates shown in figure 13 exceed the theoretical predictions which have successfully represented measurements made in coflowing mixing layers.

The authors are grateful to Dr F. Alvi for stimulating discussions on the subject of compressible shear layers and to J. King and C. Ross for assistance with the data acquisition. The research would not have been possible without the financial support of the Office of Naval Research (Grant No. N00014-92-J-1406) and the National Science Foundation (Grant No. CTS-9116532). A computing grant from the Minnesota Supercomputer Institute is also acknowledged.

REFERENCES

AKHIERZER, A. I. & POLOVIN, R. V. 1971 Criteria for wave growth. *Sov. Phys. Uspek.* **14**, 278.

ARNETTE, S. A., SAMIMY, M. & ELLIOT, G. S. 1993 On streamwise vortices in high Reynolds number supersonic axisymmetric jets. *Phys. Fluids* A **5**, 187–202.

BERMAN, C. H. & FFOWCS WILLIAMS, J. E. 1970 Instability of a two-dimensional compressible jet. *J. Fluid Mech.* **42**, 151–159.

BERS, A. 1983 Space-time evolution of plasma instabilities – absolute and convective. In *Handbook of Plasma Physics I.* (ed. M. N. Rosenbluth & R. Z. Sagdeev). North-Holland.

BIRCH, S. F. & EGGERS, J. M. 1973 A critical review of the experimental data for developed free turbulent shear layers. *NASA SP*-321, pp. 11–40.

BOGDANOFF, D. W. 1983 Compressibility effects in turbulent shear layers. *AIAA J.* **21**, 926–927.

BRIGGS, R. J. 1964 Electron-stream interaction with plasmas. *Research Monograph* 29. MIT.

BROWN, G. L. & ROSHKO, A. 1974 On density effects and large scale structure in turbulent mixing layers. *J. Fluid Mech.* **64**, 775–816.

CHINZEI, N., MASUYA, G., KOMURO, T., MURAKAMI, A. & KUDOU, K. 1986 Spreading of two-stream supersonic mixing layers. *Phys. Fluid* **29**, 1345–1347.

CHOMAZ, J. M., HUERRE, P. & REDEKOPP, L. G. 1988 Bifurcations to local and global modes in spatially-developing flows. *Phys. Rev. Lett.* **60**, 25–28.

CLEMENS, N. T. & MUNGAL, M. G. 1991 A planar Mie scattering technique for visualizing supersonic mixing flows. *Exps. Fluids* **11**, 175–185.

CLEMENS, N. T. & MUNGAL, M. G. 1992 Two- and three-dimensional effects in the supersonic mixing layer. *AIAA J.* **30**, 973–981.

ELLIOT, G. & SAMIMY, M. 1990 Compressibility effects in free shear layers. *AIAA Paper* 90-0705.

FOURGUETTE, D. C., MUNGAL, M. G. & DIBBLE, R. W. 1991 Time evolution of the shear layer of a supersonic axisymmetric jet. *AIAA J.* **29**, 1123–1130.

FREYMUTH, P. 1966 On the transition in a separated laminar boundary layer. *J. Fluid Mech.* **25**, 683–704.

GOEBEL, S. G. & DUTTON, J. C. 1991 Experimental study of compressible turbulent mixing layers. *AIAA J.* **29**, 538–546.

GROPENGIESSER, H. 1970 Study of the stability of boundary layers in compressible fluids. *NASA TT-F*-12, p. 786.

GUTMARK, E., SCHADOW, K. C. & WILSON, K. J. 1991 Effect of convective Mach number on mixing of coaxial circular and rectangular jets. *Phys. Fluids* A **3**, 29–36.

HANNEMANN, K. & OERTEL, H. 1989 Numerical simulation of the absolutely and convectively unstable wake. *J. Fluid Mech.* **199**, 55–88.

HO, C.-M. & HUERRE, P. 1984 Perturbed free shear layers. *Ann. Rev. Fluid Mech.* **16**, 365–424.

HUERRE, P. & MONKEWITZ, P. A. 1985 Absolute and convective instabilities in free shear layers. *J. Fluid Mech.* **159**, 151–168.

HUERRE, P. & MONKEWITZ, P. A. 1990 Local and global instabilities in spatially developing flows. *Ann. Rev. Fluid Mech.* **22**, 473–537.

HUMPHREY, J. A. C. & LI, S. 1981 Tilting, stretching, pairing and collapse of vortex structures in confined counter-current flows. *Trans. ASME* I: *J. Fluids Engng* **101**, 466–470.

JACKSON, T. L. & GROSCH, C. E. 1989 Inviscid spatial stability of a compressible mixing layer. *J. Fluid Mech.* **208**, 609–637.

JACKSON, T. L. & GROSCH, C. E. 1990 Absolute/convective instabilities and the convective Mach number in a compressible mixing layer. *Phys. Fluids* A **2**, 949.

JENDOUBI, S. & STRYKOWSKI, P. J. 1994 Absolute and convective instability of axisymmetric jets with external flow. *Phys. Fluids* **6**, 3000–3009.

KING, C. J., KROTHAPALLI, A. & STRYKOWSKI, P. J. 1994 Streamwise vorticity generation in supersonic jets with minimal thrust loss. *AIAA Paper* 94-0661.

KING, C. J., KROTHAPALLI, A. & STRYKOWSKI, P. J. 1995 The effect of annular counterflow on supersonic jet noise. In *Proc. 1st Joint CEAS/AIAA Aeroacoustic Conference, Munich, Germany, June 12–15*, vol. 2, pp. 1151–1158.

KOCH, W. 1985 Local instability characteristics and frequency determination of self-excited wake flows. *J. Sound Vib.* **99**, 53–83.

KROTHAPALLI, A., BUZYNA, G. & LOURENCO, L. 1991 Streamwise vortices in an underexpanded axisymmetric jet. *Phys. Fluids* A **3**, 1848–1851.

KROTHAPALLI, A., HSIA, Y., BAGANOFF, D. & KARAMCHETI, K. 1986 The role of screech tones on mixing of an underexpanded rectangular jet. *J. Sound Vib.* **106**, 119–143.

KYLE, D. & SREENIVASAN, K. R. 1993 The instability and breakdown of a round variable-density jet. *J. Fluid Mech.* **249**, 619–664.

LEPICOVSKY, J., AHUJA, K. K., BROWN, W. H., SALIKUDDIN, M. & MORRIS, P. J. 1988 Acoustically excited heated jets. *NASA CR*-4129.

MATHIS, C., PROVANSAL, M. & BOYER, L. 1984 The Bénard–von Kármán instability: an experimental study near the threshold. *J. Phys. Lett.* **45**, 483–491.

MESSERSMITH, N. L., DUTTON, J. C. & KRIER, H. 1991 Experimental investigation of large scale structure in compressible mixing layers. *AIAA Paper* 91-0244.

MICHALKE, A. 1971 Instabilität eines kompressiblen runden Freistrahls under Berücksichtigung des Einflusses der Strahlgrenzschichtdicke. *Z. Flugwiss.* **19**, 319.

MOFFETT, R. J. 1982 Contributions to the theory of single-sample uncertainty analysis. *Trans. ASME* I: *J. Fluids Engng* **104**, 250–260.

MONKEWITZ, P. A. 1988 The absolute and convective nature of instability in two-dimensional wakes at low Reynolds numbers. *Phys. Fluids* **31**, 999–1006.

MONKEWITZ, P. A., BECHERT, D. W., BARSIKOW, B. & LEHMANN, B. 1990 Self-excited oscillations and mixing in a heated round jet. *J. Fluid Mech.* **213**, 611–639.

MONKEWITZ, P. A., LEHMANN, B., BARSIKOW, B. & BECHERT, D. W. 1989 The spreading of self-excited hot jets by side jets. *Phys. Fluids* A **1**, 446–448.

MONKEWITZ, P. A. & NGUYEN, L. N. 1987 Absolute instability in the near wake of two-dimensional bluff bodies. *J. Fluids Struct.* **1**, 165–184.

MONKEWITZ, P. A. & SOHN, K. D. 1988 Absolute instability in hot jets. *AIAA J.* **26**, 911–916.

NOVOPASHIN, S. A. & PEREPELKIN, A. L. 1989 Axial symmetry loss of a supersonic preturbulent jet. *Phys. Lett.* A **135**, 290–293.

PAPAMOSCHOU, D. 1989 Structure of the compressible turbulent shear layers. *AIAA Paper* 89–0126.

PAPAMOSCHOU, D. & ROSHKO, A. 1988 The compressible turbulent mixing layer: an experimental study. *J. Fluid Mech.* **197**, 453–477.

PAVITHRAN, S. & REDEKOPP, L. G. 1989 The absolute-convective transition in subsonic mixing layers. *Phys. Fluids* A **1**, 1736–1739.

PEROOMIAN, O. & KELLY, R. E. 1994 Absolute and convective instabilities in compressible confined mixing layers. *Phys. Fluids* **6**, 3192–3194.

POWELL, A. 1953 On the mechanism of choked jet noise. *Proc. Phys. Soc. Lond.* B **66**, 1039.

RAMAN, G., HAILYE, M. & RICE, E. J. 1992 The flip flop nozzle extended to supersonic flows. *AIAA Paper* 92-2724.

RAMAN, G., RICE, E. J. & MANKBADI, R. R. 1988 Saturation and the limit of jet mixing enhancement by single frequency plane wave excitation: experiment and theory. In *Proc. AIAA/ASME/SIAM/APS 1st National Fluid Dynamics Congress*, pp. 1000–1007. ASME.

RAMSHANKAR, R. 1988 The dynamics of countercurrent mixing layers. PhD, thesis, Yale University.

ROSS, C. B., LOURENCO, L. & KROTHAPALLI, A. 1994 Particle image velocimetry measurements in a shock-containing supersonic flow. *AIAA Paper* 94-0047.

RUSS, S., STRYKOWSKI, P. J. & PFENDER, E. 1994 Mixing in plasma and low density jets. *Exps. Fluids* **16**, 297–307.

SAMIMY, M., ERWIN, D. W. & ELLIOT, G. S. 1989 Compressibility and shock wave interaction effects on free shear layers. *AIAA Paper* 89-2460.

SAMIMY, M. & LELE, S. K. 1990 Particle laden compressible free shear layers. *AIAA Paper* 90-1977.

SAMIMY, M., REEDER, M. F. & ELLIOT, G. S. 1992 Compressibility effects on large structures in free shear flows. *Phys. Fluids* **4**, 1251–1258.

SAMIMY, M., ZAMAN, K. B. M. Q. & REEDER, M. F. 1991 Supersonic jet mixing enhancement by vortex generators. *AIAA Paper* 91-2263.

SANDHAM, N. & REYNOLDS, W. C. 1990 Compressible mixing layer: linear theory and direct simulation. *AIAA J.* **28**, 618–624.

SANDHAM, N. & REYNOLDS, W. C. 1991 Three-dimensional simulations of large eddies in the compressible mixing layer. *J. Fluid Mech.* **224**, 133–158.

SCHARTON, T. D., WHITE, P. H. & RENTZ, P. H. 1973 Supersonic jet noise investigation using jet fluctuating pressure probes. *Air Force Aero Prop. Lab. Rep.* AFAPL-TR-73-35.

SCHLICHTING, H. 1978 *Boundary Layer Theory*, 7th edn. McGraw-Hill.

SHAU, Y. R. & DOLLING, D. S. 1989 Experimental study of spreading rate enhancement of high Mach number turbulent shear layers. *AIAA Paper* 89-2458.

SHAU, Y. R., DOLLING, D. S. & CHOI, K. Y. 1993 Organized structure in a compressible turbulent shear layer. *AIAA J.* **31**, 1398–1405.

SREENIVASAN, K. R., RAGHU, S. & KYLE, D. 1989 Absolute instability in variable density round jets. *Exps. Fluids* **7**, 309–317.

STRYKOWSKI, P. J. 1986 The control of absolutely and convectively unstable shear flows. PhD thesis, Yale University.

STRYKOWSKI, P. J. & KROTHAPALLI, A. 1993 The countercurrent mixing layer: strategies for shear-layer control. *AIAA Paper* 93-3260.

STRYKOWSKI, P. J., KROTHAPALLI, A. & FORLITI, D. J. 1995 Fluidic thrust vectoring of a supersonic rectangular jet using counterflow. *AIAA J.* (under review).

STRYKOWSKI, P. J., KROTHAPALLI, A. & WISHART, D. 1993 Enhancement of mixing in high-speed heated jets using a counterflowing nozzle. *AIAA J.* **31**, 2033–2038.

STRYKOWSKI, P. J. & NICCUM, D. L. 1991 The stability of countercurrent mixing layers in circular jets. *J. Fluid Mech.* **227**, 309–343.

STRYKOWSKI, P. J. & NICCUM, D. L. 1992 The influence of velocity and density ratio on the dynamics of spatially developing mixing layers. *Phys. Fluids* A **4**, 770–781.

STRYKOWSKI, P. J. & WILCOXON, R. K. 1993 Mixing enhancement due to global oscillations in jets with annular counterflow. *AIAA J.* **31**, 564–570.

THORPE, A. S. 1968 A method of producing a shear flow in a stratified fluid. *J. Fluid Mech.* **32**, 693–704.

THORPE, A. S. 1971 Experiments on instability and turbulence in a stratified shear flow: miscible fluids. *J. Fluid Mech.* **46**, 299–319.

YU, K., GUTMARK, E. & SCHADOW, K. C. 1993 Passive control of coherent vortices in compressible mixing layers. *AIAA Paper* 93-3262.

YU, K., KRAEUTLE, K., WILSON, K., PARR, T., SMITH, R., GUTMARK, E. & SHADOW, K. C. 1992 Supersonic flow mixing and combustion using a ramp nozzle. *AIAA Paper* 92-3840.

ZAPRYAGAEV, V. I. & SOLOTCHIN, A. V. 1988 Spatial structure of flow in the initial section of a supersonic underexpanded jet. *Acad. Sci. USSR*, No. 23–88.